Resonance Theory of Vibrational Polariton Chemistry

Wenxiang Ying,*,† Michael A.D. Taylor,‡ and Pengfei Huo*,†,‡

†*Department of Chemistry, University of Rochester, 120 Trustee Road, Rochester, New York 14627, USA*

‡*Institute of Optics, Hajim School of Engineering, University of Rochester, Rochester, New York, 14627, USA*

E-mail: wying3@ur.rochester.edu; pengfei.huo@rochester.edu

Abstract

We present a theory that explains the vibrational strong coupling (VSC) modified reaction rate constant. This analytic theory is based on a mechanistic hypothesis that cavity modes promote the transition from the ground state to the vibrational excited state of the reactant, which is the rate-limiting step of the reaction. Using Fermi's Golden Rule, we can formulate this rate constant for many molecules collectively coupled to many cavity modes inside a Fabry-Pérot microcavity. The theory clearly explains the resonance condition for the observed VSC effect and provides the first-ever explanation of why only at the normal incident angle there is the resonance effect, due to a van-Hove-type singularity in the density of states for the photonic modes. Assuming the coherent vibrational energy transfer picture and for aligned dipoles, the theory can also explain the collective effect and makes several experimentally verifiable predictions. However, by assuming an incoherent picture of vibrational energy transfer, the theory cannot explain the collective effect.

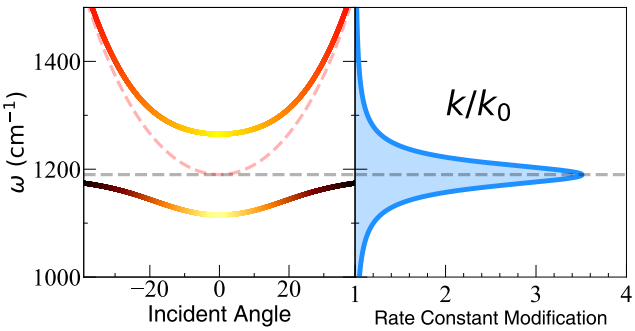

Recent experiments[1–6] have demonstrated that chemical reaction rate constants can be suppressed[1–4,7–9] or enhanced[5,6,10] by resonantly coupling molecular vibrations to quantized radiation modes inside a Fabry-Pérot (FP) microcavity.[11–13] This effect has the potential to selectively slow down competing reactions[3] or speed up a target reaction, thus achieving mode selectivity and offering a paradigm shift in chemistry. Despite extensive theoretical efforts,[8,14–41] the fundamental mechanism and theoretical understanding of the cavity-modified ground-state chemical kinetics remain elusive.[14,42–44] To the best of our knowledge, there is no unified theory that can explain all of the observed phenomena in the vibrational strong coupling (VSC) experiments,[14] including (1) The resonance effect, which happens when the cavity frequency matches the bond vibrational frequency, $\omega_c = \omega_0$, but also only happens when the in-plane photon momentum is $k_{\parallel} = 0$, (2) The collective effect, which is the increase in the *magnitude* of VSC modification when increasing the number of molecules N (or concentration $N/\mathcal{V}$),[1,4,5] (3) The driving by thermal fluctuations without optical pumping.[1,3] (4) The isotropic disorder of dipoles in the cavity, which is assumed of experiments with many molecules.[14]

We aim to develop a microscopic theory to explain these observed VSC effects. Let us consider N identical molecules coupled to many radiation

modes inside a Fabry-Pérot cavity,

$$\hat{H} = \sum_{j=1}^{N} \frac{\hat{P}_j^2}{2M} + V(\hat{R}_j) + \hat{H}_\nu + \hat{H}_{\text{loss}}(\hat{q}_{\mathbf{k}}, \hat{x}_{\mathbf{k},\zeta}) + \sum_{\mathbf{k}} \frac{\hat{p}_{\mathbf{k}}^2}{2} + \frac{\omega_{\mathbf{k}}^2}{2}\left(\hat{q}_{\mathbf{k}} + \frac{\lambda_c}{\omega_{\mathbf{k}}} \cdot \sum_{j=1}^{N} \mu(\hat{R}_j) \cdot \cos\varphi_j\right)^2, \tag{1}$$

where $\hat{R}_j$ is the reaction coordinate for the j_{th} molecule, $V(\hat{R}_j)$ is the ground state potential for each reaction molecule (a double well potential for this paper as is typical for VSC simulations[22,27,34,39]), and $\mu(\hat{R}_j)$ is the dipole associated with the ground electronic state (electronic permanent dipole).

The Fabry-Pérot cavity has the following dispersion relation,

$$\omega_{\mathbf{k}}(k_\parallel) = \frac{c}{n_c}\sqrt{k_\perp^2 + k_\parallel^2} = \frac{ck_\perp}{n_c}\sqrt{1+\tan^2\theta}, \tag{2}$$

where c is the speed of light, n_c is the refractive index of the cavity, and θ (usually referred to as the incident angle) is the angle of the photonic mode wavevector, $\mathbf{k}$, relative to the norm direction of the mirrors. When $k_\parallel = 0$ (or $\theta = 0$), the photon frequency is

$$\omega_c \equiv \omega_{\mathbf{k}}(k_\parallel = 0) = ck_\perp/n_c. \tag{3}$$

The cavity frequency $\omega_{\mathbf{k}}$ in Eq. 1 is associated with the wavevector $\mathbf{k}$, according to Eq. 2. Furthermore, $\hat{q}_{\mathbf{k}} = \sqrt{\hbar/(2\omega_{\mathbf{k}})}(\hat{a}_{\mathbf{k}}^\dagger + \hat{a}_{\mathbf{k}})$ and $\hat{p}_{\mathbf{k}} = i\sqrt{\hbar\omega_{\mathbf{k}}/2}(\hat{a}_{\mathbf{k}}^\dagger - \hat{a}_{\mathbf{k}})$, $\hat{a}_{\mathbf{k}}$ and $\hat{a}_{\mathbf{k}}^\dagger$ are the photonic field annihilation and creation operators for mode $\mathbf{k}$, respectively. The light-matter coupling strength is $\lambda_c = \sqrt{1/(\epsilon_0 \mathcal{V})}$, where ϵ_0 is the effective permittivity inside the cavity and $\mathcal{V}$ is the cavity quantization volume. Each reaction coordinate R_j is coupled to its own local phonon bath described by $\hat{H}_\nu$. Each cavity mode $\hat{q}_{\mathbf{k}}$ couples to its independent bath $\{\hat{x}_{\mathbf{k},\zeta}\}$, accounting for the cavity loss. The cavity modes $\{\hat{q}_{\mathbf{k}}\}$ couple to the dipole of each molecule $\mu(\hat{R}_j)$, where φ_j is the relative angle between the dipole vector and the field polarization direction. Details of the Hamiltonian are provided in Supporting Information, Sec. I.

Fig. 1 presents the first few vibrational states of the double well model, where $|\nu_L\rangle$ denotes the vibrational ground state of the reactant (left well), $|\nu'_L\rangle$ denotes the vibrationally excited state of the reactant, and similar for the product (right well).

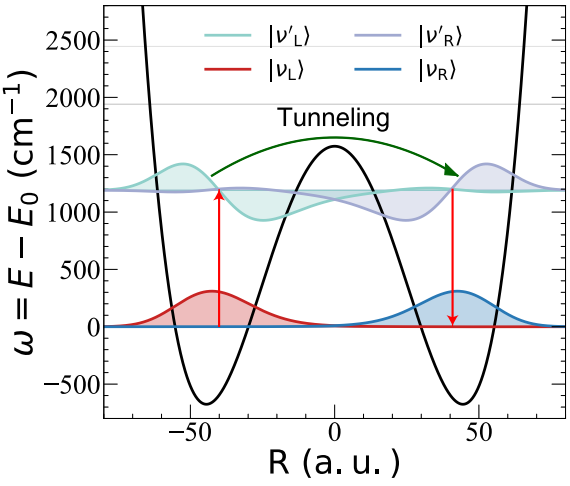

Figure 1: Potential energy surface for the reaction model.[39] The red arrows represent the thermal activation process from the vibrational ground state, $|\nu_L\rangle$, to the vibrationally excited state, $|\nu'_L\rangle$ in the reactant well (left side of the barrier). Then through the coupling between $|\nu'_L\rangle$ and $|\nu'_R\rangle$, a chemical reaction occurs. Finally, the vibrational excited state $|\nu'_R\rangle$ relaxed to the ground state $|\nu_R\rangle$. The presence of the cavity mode $\hat{q}_{\mathbf{k}}$ can be viewed as the rate-promoting mode, that explicitly enhances the transition $|\nu_L\rangle \to |\nu'_L\rangle$.

The red arrow represents the thermal activation process from the vibrational ground state, $|\nu_L\rangle$, to the vibrationally excited state, $|\nu'_L\rangle$ in the reactant well. Then, through the coupling between $|\nu'_L\rangle$ and $|\nu'_R\rangle$, a chemical reaction occurs. Finally, the vibrational excited state $|\nu'_R\rangle$ relaxes to the ground state of the product $|\nu_R\rangle$. The presence of the cavity mode $\hat{q}_{\mathbf{k}}$ can be viewed as the rate-promoting mode, which explicitly enhances the transition $|\nu_L\rangle \to |\nu'_L\rangle$. The symmetric double-well model[39] is used to model the reaction, with details in Supporting Information, Sec II.

Let us consider a simplified reaction mechanism outside the cavity as $|\nu_L\rangle \xrightarrow{k_1} |\nu'_L\rangle \xrightarrow{k_2} |\nu'_R\rangle \xrightarrow{k_3} |\nu_R\rangle$. Note that this is the quantum description of the reaction based on quantized states, whereas the classical description is a barrier crossing along the reaction coordinate. These vibrational diabatic states can be directly obtained by computing the eigenspectum of $V(\hat{R})$ and then diabatizing it. The simplified mechanism for the reaction is that the thermal activation process causes the transition of $|\nu_L\rangle \to |\nu'_L\rangle$. Then the reaction occurs through the diabatic couplings between $|\nu'_L\rangle$ and $|\nu'_R\rangle$, followed by a vibrational relaxation of the product state, $|\nu'_R\rangle \to |\nu_R\rangle$. The rate-limiting step for the entire process is k_1, where $k_2 \gg k_1$ such that the

populations of both $|\nu'_{\rm L}\rangle$ and $|\nu'_{\rm R}\rangle$ reach a steady state (plateau in time), and from the steady-state approximation, the overall rate constant for the reaction is $k_0 \approx k_1$.

Considering many molecules, we focus on the single excitation subspace. This includes the ground state $|G\rangle$ and N singly excited states $|\nu_j\rangle$ (where $j \in [1, N]$ labels the molecules), defined as

$$|G\rangle \equiv |\nu^1_{\rm L}\rangle ... \otimes ... |\nu^j_{\rm L}\rangle \otimes ... |\nu^N_{\rm L}\rangle, \tag{4a}$$

$$|\nu_j\rangle \equiv |\nu^1_{\rm L}\rangle ... \otimes ... |\nu'^j_{\rm L}\rangle \otimes ... |\nu^N_{\rm L}\rangle. \tag{4b}$$

The vibrational transition dipole matrix element is

$$\mu_{\rm LL'} = \langle \nu'^j_{\rm L} | \mu(\hat{R}_j) | \nu^j_{\rm L} \rangle, \tag{5}$$

which is identical for all molecules j. When measuring the absorption spectra of the molecule, the optical response shows a peak at the quantum vibrational frequency $\omega_0 = (E_{\rm L'} - E_{\rm L})/\hbar$.

In the singly excited manifold, the collective "bright state" is defined as $|{\rm B}\rangle = \frac{1}{\sqrt{N}} \sum_{k=1}^{N} |\nu_k\rangle$. The light-matter coupling term, $\propto \sum_{\mathbf{k},j} \hat{q}_{\mathbf{k}} \otimes \mu(\hat{R}_j)$ in Eq. 1, will hybridize the bright state and photon-dressed ground states, generating polariton states.[45] When all dipoles are fully aligned, such that $\cos\varphi_j = 1$, and under the resonance condition $\omega_{\mathbf{k}}(k_\parallel) = \omega_0$, the light-matter hybridization generates the upper and lower polariton states[46] as $|\pm_{\mathbf{k}}\rangle = \frac{1}{\sqrt{2}}[|{\rm B}\rangle \otimes |0_{\mathbf{k}}\rangle \pm |G\rangle \otimes |1_{\mathbf{k}}\rangle]$ (which are light-matter entangled states) where $|0_{\mathbf{k}}\rangle$ and $|1_{\mathbf{k}}\rangle$ are photonic Fock states corresponding to the mode with the wavevector, $\mathbf{k}$. The Rabi splitting is

$$\Omega_{\rm R} = \sqrt{\frac{2\omega_{\mathbf{k}}}{\hbar\epsilon_0}} \sqrt{\frac{N}{\mathcal{V}}} \mu_{\rm LL'} \equiv 2\sqrt{N} g_{\rm c} \cdot \sqrt{\omega_{\mathbf{k}}}, \tag{6}$$

where $g_{\rm c} = \mu_{\rm LL'} \sqrt{1/(2\hbar\epsilon_0 \mathcal{V})}$ is the Jaynes-Cummings[47] type coupling strength (without the $\sqrt{\omega_{\mathbf{k}}}$-dependence). There are also $N-1$ dark states that do not mix with the photonic degrees of freedom (DOF) under this approximation. Details of this standard analysis are provided in the Supporting Information, Sec. III. The formation of Rabi splitting/polariton states comes from a collective phenomenon, resulting in the well-known dependence of $\sqrt{N}$ or equivalently $\sqrt{N/\mathcal{V}}$ for $\Omega_{\rm R}$, which has been experimentally confirmed.[4] It has been estimated that there are $N \sim 10^6 - 10^{12}$ molecules effectively coupled to the cavity mode[14,16,48] for the recent VSC experiments,[1,4] and $\Omega_{\rm R} \sim 100$ cm^{-1} when $\omega_0 \approx 1000$ cm^{-1} for typical VSC experiments.[4,5] What remains largely a mystery is why the delocalized light-matter hybridization can influence chemical reaction rate constant, when a reaction is often thought of as a local phenomenon that involves breaking a bond in a molecule.[14] In addition, the entire device is kept under dark conditions such that there is no additional optical pumping.[11,12,14] As such, Ebbesen and co-workers hypothesized that the fundamental mechanism of VSC must be related to the quantum field vacuum fluctuations.[1,3]

To provide a microscopic mechanism of VSC-modified reactions, we *hypothesize* that the cavity modes enhance the transition from ground states to a vibrationally excited state manifold of the reactant, leading to an enhancement of the *steady-state population* of both the delocalized states on the reactant side and the excited states manifold on the product side (right well) $\{|\nu'^j_{\rm R}\rangle\}$, which then relax to the vibrational ground state manifold on the product side (right well), $\{|\nu^j_{\rm R}\rangle\}$. The proposed mechanism is outlined as follows,

$$|G\rangle \xrightarrow{k_1} \{|\nu'^j_{\rm L}\rangle\} \xrightarrow{k_2} \{|\nu'^j_{\rm R}\rangle\} \xrightarrow{k_3} \{|\nu^j_{\rm R}\rangle\}. \tag{7}$$

When the molecular system is originally in the Kramers low friction regime (before the Kramers turnover,[49,50] or so-called the energy diffusion-limited regime), the cavity enhancement of the rate constant k_1 will occur.[30–32,34,35,39] When explicitly assuming that $k_1 \ll k_2, k_3$, then $|G\rangle \xrightarrow{k_1} \{|\nu'^j_{\rm L}\rangle\}$ is the *rate limiting step*, and the population of the intermediate states will reach a steady-state behavior. As such, because of the steady-state approximation, the overall rate constant is

$$k \approx k_1 = k_0 + k_{\rm VSC} \ll k_2, k_3, \tag{8}$$

where k_0 is the chemical reaction rate constant outside the cavity, and $k_{\rm VSC}$ accounts for the pure cavity-induced effect. Note that Eq. 8 assumes that the pure cavity effect $k_{\rm VSC}$ can be added with k_0, which is a *fundamental assumption* in the current theory.

To quantitatively express $k_{\rm VSC}$, we analyze the overall effect of the cavity and the photon-loss environment on the molecular systems by performing a normal mode transformation[51–53] to the Hamiltonian in Eq. 1 and obtaining an effective Hamiltonian, where now the cavity modes $\{\hat{q}_{\mathbf{k}}\}$ and the photon-loss bath modes $\{\hat{x}_{\mathbf{k},\zeta}\}$ (described by $\hat{H}_{\rm loss}$) are transformed into effective photonic nor-

mal mode coordinates $\{\hat{\tilde{x}}_{\mathbf{k},\zeta}\}$, that are collectively coupled to the system DOFs through the following term,

$$\hat{H}_{\mathrm{LM}} = \hat{\mathcal{S}} \otimes \hat{F}_{\mathrm{eff}}, \tag{9}$$

where $\hat{\mathcal{S}} \equiv \sum_{j=1}^{N} \mu(\hat{R}_j) \cdot \cos\varphi_j$ is the collective system operator, $\hat{F}_{\mathrm{eff}} = \sum_{\mathbf{k},\zeta} \tilde{c}_{\mathbf{k},\zeta} \hat{\tilde{x}}_{\mathbf{k},\zeta}$ is the stochastic force exerted by the effective bath, $\{\hat{\tilde{x}}_{\mathbf{k},\zeta}\}$ are the normal modes of $\{\hat{q}_{\mathbf{k}}, \hat{x}_{\mathbf{k},\zeta}\}$, and the coupling constants $\tilde{c}_{\mathbf{k},\zeta}$ as well as bath frequencies $\tilde{\omega}_{\mathbf{k},\zeta}$ are characterized by an effective spectral density,

$$J_{\mathrm{eff}}(\omega) = \sum_{\mathbf{k}} \frac{\lambda_{\mathrm{c}}^2 \omega_{\mathbf{k}}^2 \tau_{\mathrm{c}}^{-1} \omega}{\left(\omega_{\mathbf{k}}^2 - \omega^2\right)^2 + \tau_{\mathrm{c}}^{-2} \omega^2}, \tag{10}$$

where τ_{c} is the cavity lifetime. See Supporting Information, Sec. IV. Under the continuous $k_{\parallel}$ limit, one can replace the sum with an integral, $\sum_{\mathbf{k}} f(\mathbf{k}) \to \int dk g(k) f(k)$, where $g(k)$ is the density of states (DOS) for the modes according to the dispersion relation in Eq. 2. One can further show that the DOS for the photonic modes is expressed as

$$g(\theta) = \frac{1}{2k_{\perp} \tan\theta_{\mathrm{m}}} \sqrt{1 + \cot^2\theta}, \tag{11}$$

for $\theta_{\mathrm{m}} \leq \theta \leq \theta_{\mathrm{m}}$, where θ_{m} is the maximum incident angle. The DOS, $g(\theta)$, in Eq. 11 has a singularity at $\theta = 0$, which is known as a Van-Hove type singularity.[54] Using the above DOS and replacing the sum in Eq. 10 as an integral, we have

$$J_{\mathrm{eff}}(\omega) \tag{12}$$
$$= \frac{\omega_{\mathrm{c}}^2 \lambda_{\mathrm{c}}^2}{\tan\theta_{\mathrm{m}}} \int_0^{\theta_{\mathrm{m}}} d\theta \, \frac{\sqrt{1 + \cot^2\theta}}{\cos^4\theta} \frac{\tau_{\mathrm{c}}^{-1} \omega}{\left(\omega_{\mathbf{k}}^2 - \omega^2\right)^2 + \tau_{\mathrm{c}}^{-2} \omega^2},$$

where $\omega_{\mathbf{k}}^2 = \omega_{\mathrm{c}}^2 (1 + \tan^2\theta)$. By taking the limit of $\theta_{\mathrm{m}} \to \pi/2$ and evaluating the integral (which gives a finite value despite the singularity in $g(\theta)$), only the contribution from $\theta = 0$ survives, which gives the following closed analytic expression,

$$J_{\mathrm{eff}}(\omega) = \lambda_{\mathrm{c}}^2 \omega_{\mathrm{c}}^2 \frac{\tau_{\mathrm{c}}^{-1} \omega}{\left(\omega_{\mathrm{c}}^2 - \omega^2\right)^2 + \tau_{\mathrm{c}}^{-2} \omega^2}. \tag{13}$$

The details of the derivations are provided in the Supporting Information, Sec. V. The above theoretical results also formally justify the commonly used single mode approximation in investigating VCS reactivities,[22,27,39] because only the mode with the frequency ω_{c} survives in $J_{\mathrm{eff}}(\omega)$.

The rate constant change k_{VSC} in Eq. 8 originates from a purely cavity-induced effect, causing the promotion of the transition from $|G\rangle$ to the singly excited states manifold $\{|\nu_j\rangle\}$. Note that the light-matter coupling term in Eq. 9 suggests that through the collective coupling between all molecules and the cavity modes, the cavity operator $\hat{F}_{\mathrm{eff}}$ will mediate the transition. We use Fermi's golden rule (FGR) to estimate this transition rate constant. The coupling for this quantum transition is provided by $\hat{\mathcal{S}}$, and the transition is mediated by the effective photon bath operator $\hat{F}_{\mathrm{eff}}$ with its spectral density $J_{\mathrm{eff}}(\omega)$ in Eq. 12. Since $\hat{H}_{\mathrm{LM}}$ from Eq. 9 is a *non-local* operator that couples the molecules to the cavity, we hypothesize that the transitions of $|G\rangle \to |\nu_L'^j\rangle$ are not independent pathways. As such, in FGR one needs to explicitly account for the interference of pathways[55] such that one must add them together before squaring them in the FGR. This is the coherent picture of FGR,[36] which gives

$$k_{\mathrm{VSC}} = \frac{1}{N} \frac{2}{\hbar} \left| \left(\sum_{k=1}^{N} \langle \nu_k | \hat{\mathcal{S}} | G \rangle \right) \right|^2 \cdot J_{\mathrm{eff}}(\omega_0) \cdot n(\omega_0), \tag{14}$$

where the $1/N$ factor accounts for the normalized rate constant per molecule, as we are considering the collective transition along N molecules between $|G\rangle$ and $\{|\nu_j\rangle\}$. Further, $n(\omega_0) = 1/(e^{\beta\hbar\omega_0} - 1) \approx e^{-\beta\hbar\omega_0}$ (when $\beta\hbar\omega_0 \gg 1$ for $\omega_0 \approx 1200$ cm^{-1} and room temperature $1/\beta = k_{\mathrm{B}}T \approx 200$ cm^{-1}, where k_{B} is the Boltzmann constant).

If we assume the pathways are completely independent, *i.e.*, the incoherent picture, the FGR rate will be expressed as

$$k_{\mathrm{VSC}} = \frac{1}{N} \frac{2}{\hbar} \sum_{k=1}^{N} \left| \langle \nu_k | \hat{\mathcal{S}} | G \rangle \right|^2 \cdot J_{\mathrm{eff}}(\omega_0) \cdot n(\omega_0), \tag{15}$$

which simply sums up each pathway's contribution. We will see that the resonance condition (related to $J_{\mathrm{eff}}(\omega_0)$) naturally shows up, regardless of the coherent or incoherent picture, but the collective effect only survives for the coherent picture when dipoles are fully aligned with cavity field polarization.

Resonance effect. Let us first focus on the resonance effect, which should be explained by $J_{\mathrm{eff}}(\omega_0)$ term in k_{VSC}, regardless of the coherent or incoherent picture. More specifically, $J_{\mathrm{eff}}(\omega_0)$ is

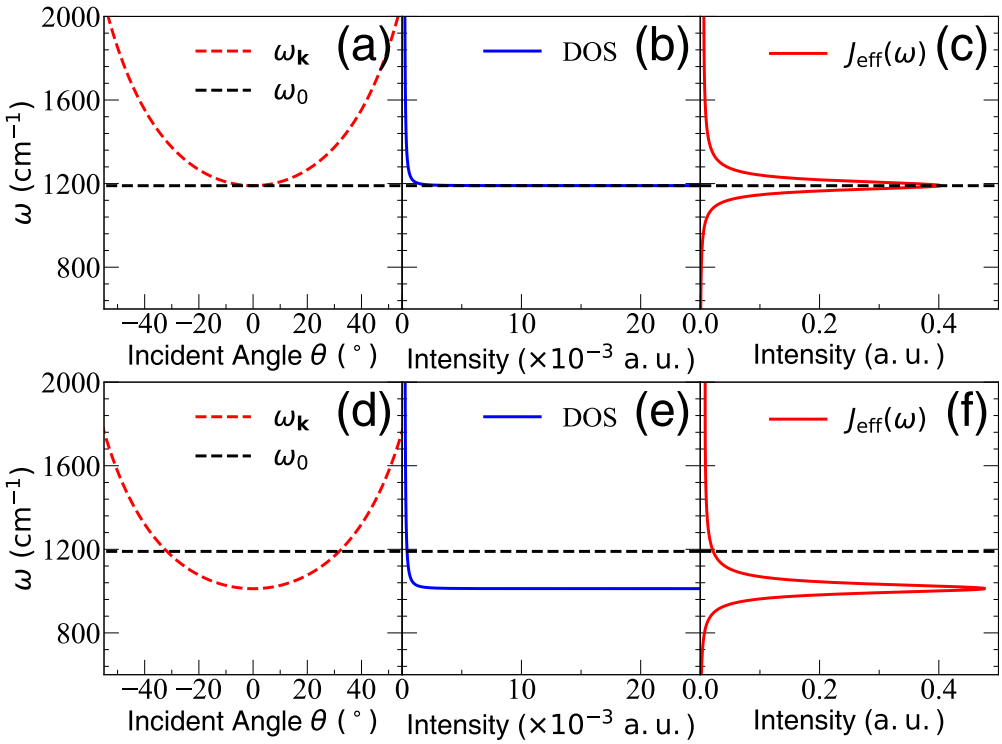

Figure 2: (a) The cavity dispersion relation (Eq. 2), (b) the density of states $g(\theta)$ (Eq. 11), and (c) effective spectral density function $J_{\text{eff}}(\omega)$ (Eq. 13) for the normal incidence case $\omega_c = \omega_0$, where the resonance condition is reached at $\theta = 0$. (d)-(f) correspond to the red-detuned case (oblique incidence), with $\omega_c = 0.85\ \omega_0$, whose resonance condition is reached at around $\theta = 32°$. The cavity lifetime is taken as $\tau_c \approx 106$ fs.

expressed as follows,

$$J_{\text{eff}}(\omega_0) = \lambda_c^2 \omega_c^2 \frac{\tau_c^{-1}\omega_0}{\left(\omega_c^2 - \omega_0^2\right)^2 + \tau_c^{-2}\omega_0^2}. \tag{16}$$

It is self-evident that the peak of this function is located at $\omega_c = \omega_0$ for $k_{\parallel} = 0$, agreeing with experimental observations.[1,11–13] Thus, the VSC-modified rate constant only occurs when $\omega_c = \omega_0$. This is because there is a Van-Hove type singularity[54] in the density of states, $g(\theta)$, which manifests itself as the $\sqrt{1+\cot^2\theta}$ term in Eq. 12, such that the integral only survives and gives a finite value at $\theta = 0$, and at $\theta > 0$, the integral becomes vanishingly small.

To illustrate this, Fig. 2 presents the cavity dispersion relation of $\omega_{\mathbf{k}}(\theta)$ (see Eq. 2) in panels (a) and (d), the density of states (Eq. 11) in panels (b) and (e), and the effective spectral density function $J_{\text{eff}}(\omega)$ (see Eq. 13) in panels (c) and (f). One can clearly see that under the normal incident condition in panels (a)-(c) when $\theta = 0$, $J_{\text{eff}}(\omega)$ is maximized at $\omega_c = \omega_0$ and accordingly, the rate constant will also maximize based on the FGR expression (Eq. 14 or Eq. 15). At the detuned case ($\omega_c \neq \omega_0$ or $|\theta| > 0$) in panels (d)-(f), the intensity of $J_{\text{eff}}(\omega)$ still peaks at $\theta = 0$, but the intensity of $J_{\text{eff}}(\omega_0)$ diminishes at the "resonance condition" $\omega_{\mathbf{k}} = \omega_0$ (for generating Rabi splitting). This explains the experimentally observed resonance phenomena[11,14] which only occur at $\omega_c = \omega_0$ at the normal incident angle when $k_{\parallel} = 0$ (or $\theta = 0$).

The condition for observing the Rabi splitting, on the other hand, is $\omega_{\mathbf{k}}^2 = \omega_c^2(1+\tan^2\theta) = \omega_0^2$ for any $\theta \geq 0$. Although those modes with $\theta > 0$ do not contribute to k_{VSC}, the mode density is *finite* (see Fig. 2e) and for $\omega_0 > \omega_c$ there will *always* be a mode available that satisfies $\omega_{\mathbf{k}} = \omega_0$, generating Rabi splitting at $\theta > 0$. As such, we provided a clear understanding of the fundamental difference between the condition for forming Rabi splitting and that of the VSC resonance modification of the rate constant. To the best of our knowledge, this is the first theory that provides a clear understanding of the resonance condition at $k = 0$ that agrees with the experimental observation.[14]

Collective Effect. We begin by considering the coherent FGR in Eq. 14. If all the molecules' dipoles are perfectly aligned with the cavity TE polarization, then $\cos\varphi_j = 1$ for all molecules, j,

and $\hat{\mathcal{S}} = \sum_j \mu(\hat{R}_j)$. Evaluating Eq. 14 leads to

$$k_{\rm VSC} = \frac{2}{\hbar} N \mu_{\rm LL'}^2 \cdot J_{\rm eff}(\omega_0) \cdot n(\omega_0) \tag{17}$$
$$= 4N g_{\rm c}^2 \omega_{\rm c}^2 \cdot \frac{\tau_{\rm c}^{-1}\omega_0}{\left(\omega_{\rm c}^2 - \omega_0^2\right)^2 + \tau_{\rm c}^{-2}\omega_0^2} \cdot e^{-\beta\hbar\omega_0},$$

where in the second line we have explicitly approximated $n(\omega_0) \approx e^{-\beta\hbar\omega_0}$. As a special case, when $\omega_{\rm c} = \omega_0$, Eq. 17 becomes

$$k_{\rm VSC} = \Omega_{\rm R}^2 \cdot \tau_{\rm c} \cdot e^{-\beta\hbar\omega_0}, \tag{18}$$

where $\Omega_{\rm R} = 2\sqrt{N} g_{\rm c} \cdot \sqrt{\omega_0}$. The cavity quality factor is often defined as $Q = \tau_{\rm c}^{-1}\omega_0$ for the resonance condition. For the recent VSC experiment by Ebbesen,[3] the typical values for these parameters are $\tau_{\rm c} \approx 100$ fs (reading from a width of $\Gamma_{\rm c} = \tau_{\rm c}^{-1} \approx 53$ cm^{-1} of the cavity transmission spectra). If the cavity frequency $\omega_{\rm c} = \omega_0 = 1200$ cm^{-1}, then the quality factor is $Q \approx 22.6$. The coherent FGR theory predicts the resonance effect ($\omega_{\rm c} = \omega_0$) with the requirement of $k_\parallel = 0$ and the collective effect ($k_{\rm VSC} \propto N g_{\rm c}^2$). The mechanism for the VSC modification is governed by thermal activation ($\propto e^{-\beta\hbar\omega_0}$). For the incoherent theory in Eq. 15, $k_{\rm VSC}$ will have an identical expression of Eq. 17, with the only difference being without N. The rate under the resonance condition in Eq. 18, on the other hand, remains the same, with $\Omega_{\rm R}^2$ generated with large $g_{\rm c}$ instead of through the collective effect with $\sqrt{N}$.

If we consider the fully isotropically disordered dipoles (which is assumed to be the case for most of the VSC experiments[14]), such that under an ensemble average, the angle distribution becomes $\langle \cos\varphi_j \cos\varphi_k \rangle = \frac{1}{3}\delta_{jk}$, then the ensemble average of the coupling square matrix elements become $\langle (\sum_{k=1}^N \langle \nu_k | \hat{\mathcal{S}} | G \rangle |)^2 \rangle = \mu_{\rm LL'}^2 \langle |\sum_j \cos\varphi_j|^2 \rangle = \mu_{\rm LL'}^2 \cdot N/3$, which will not give rise to any collective enhancement due to the normalization term $1/N$ in Eq. 14. Similarly, classical VSC theories[21,27,32] found the same diminishing modification when considering a fully isotropic dipole distribution. Alternatively, if one considers the incoherent picture in Eq. 15, the current theory can not predict any collective effect either. Connecting to the recent theory development on polariton mediated exciton energy transfer,[36] the fully aligned dipole case is equivalent to the coherent pathway picture and the case of the fully isotropic dipoles corresponds to the incoherent picture.[36] In order to explain non-vanishing results for the isotropic dipoles, one either has to introduce new physics beyond what we have considered here or acknowledge that $\langle \cos\varphi_j \cos\varphi_k \rangle = \frac{1}{3}\delta_{jk}$ is not the case inside the cavity.[56] This is subject to future investigations. Note that the validity of the resonance effect (in Eq. 16) remains regardless of the assumption of the coherent picture in Eq. 14.

For the subsequent steps of the reaction $\{|\nu_{\rm L}'^j\rangle\} \xrightarrow{k_2} \{|\nu_{\rm R}'^j\rangle\}$, coupling to the cavity should not cause any *additional* influence on k_2, due to the local nature of chemistry. A simple argument is provided in Supporting Information, Sec. II. For typical VSC experiments,[1,4–6,8] the maximum rate change is ~ 5 times compared to the outside cavity case.[11] As long as $k_2 > k_1 \approx 5k_0$, k_2 will not become a bottleneck that ruins the steady-state approximation. Considering that the excited state tunneling is usually fast due to the large overlap between the $|\nu_{\rm L}'\rangle$ and $|\nu_{\rm R}'\rangle$ (that gives rise to tunneling coupling), this is a reasonable assumption of the conjectured mechanism in Eq. 7. Similarly, for the final step, $\{|\nu_{\rm R}'^j\rangle\} \xrightarrow{k_3} \{|\nu_{\rm R}^j\rangle\}$ there is no additional cavity modification (if the product is not coupled to the cavity).

Rate constant for the high $\tau_{\rm c}$ limit. Note that Eq. 14 is only valid for the low $\tau_{\rm c}$ limit. For $\tau_{\rm c} \to \infty$ limit, Eq. 14 will diverge due to the infinitely narrow $J_{\rm eff}(\omega_0)$. The actual VSC-modified rate constant, however, will not diverge due to the phonon broadening (from the $\hat{H}_\nu$ term in Eq. 1). By analyzing the role of the phonon coupling (see Supporting Information, Sec. VI), the VSC-modified rate constant is expressed as

$$\tilde{k}_{\rm VSC} = \int_0^\infty d\omega \; k_{\rm VSC}(\omega) G(\omega - \omega_0), \tag{19}$$

where $k_{\rm VSC}(\omega)$ is expressed in Eq. 17, $G(\omega - \omega_0) = \frac{1}{\sqrt{2\pi\sigma^2}} \exp\left[-(\omega-\omega_0)^2/2\sigma^2\right]$ is a Gaussian broadening function, with the width controlled by the phonon broadening

$$\sigma^2 = \epsilon_z^2 \cdot \frac{1}{\pi} \int_0^\infty d\omega \; J_\nu(\omega) \coth(\beta\omega/2), \tag{20}$$

where $\epsilon_z = \langle \nu_{\rm L}' | \hat{R}_j | \nu_{\rm L}' \rangle - \langle \nu_{\rm L} | \hat{R}_j | \nu_{\rm L} \rangle$ (for every molecule, j). Under the limit when the phonon broadening is much smaller than the cavity-induced broadening, which occurs when $\tau_{\rm c}^{-1} \gg \sigma$ (for example, when $\tau_{\rm c} \to 0$), the Gaussian function G is then much narrower than $J_{\rm eff}(\omega)$, so we can approximate $G(\omega - \omega_0)$ as a single δ-function,

$G(\omega-\omega_0)\approx\delta(\omega-\omega_0)$. Then, $\tilde{k}_{\rm VSC}\approx k_{\rm VSC}(\omega_0)$, and Eq. 19 reduces to Eq. 14. The detailed derivation of Eq. 19 is provided in the Supporting Information, Sec. VI.

Under the limit that $\tau_{\rm c}^{-1}\ll\sigma$, $J_{\rm eff}(\omega)\approx\frac{\pi}{2}\lambda_{\rm c}^2\omega_{\rm c}\delta(\omega-\omega_{\rm c})$, and Eq. 17 reduces to

$$\tilde{k}_{\rm VSC}\approx 2\pi N g_{\rm c}^2\omega_{\rm c}\cdot G(\omega_{\rm c}-\omega_0)\cdot e^{-\beta\hbar\omega_0}, \qquad (21)$$

where the Gaussian function gives the resonance effect. Details of derivation, as well as the numerical behavior of Eq. 19 (see Fig. S1), are provided in Supporting Information, Sec. VI - VII.

Reaction Rate. The reaction rate for the system is $\mathcal{R}=(k_0+k_{\rm VSC})\cdot N$. For the coherent FGR (Eq. 17), the rate is expressed as

$$\mathcal{R}=Nk_0+4N^2g_{\rm c}^2\omega_{\rm c}^2\cdot\frac{\tau_{\rm c}^{-1}\omega_0}{\left(\omega_{\rm c}^2-\omega_0^2\right)^2+\tau_{\rm c}^{-2}\omega_0^2}\cdot e^{-\beta\hbar\omega_0}, \qquad (22)$$

which predicts a fundamental change in the scaling with respect to the number of molecules (concentration). Note that not to be confused between the content of rate $\mathcal{R}$ and rate constant k (per molecule rate). Outside the cavity, $k_{\rm VSC}=0$, such that $\mathcal{R}=k_0\cdot N$ for the simple unimolecular reaction we considered here. By coupling to the optical cavity, if $k_0\ll k_{\rm VSC}$, the reaction rate scales as $\mathcal{R}\propto N^2$ as long as the steady-state approximation is valid. In the recent VSC-enhanced experiments, one does observe that (for example, Fig. 4b in Ref. 10) $\mathcal{R}$ changes the scaling with respect to N from a linear dependence (outside the cavity) to a non-linear dependence of N (inside the cavity). For incoherent FGR (Eq. 15), the rate $\mathcal{R}$ will scale linearly with N inside the cavity. If $g_{\rm c}$ is negligibly small, then the incoherent FGR theory predicts that there is no apparent change in the rate.

Numerical Results. We adopt a simple model system, as in Ref. 39, to illustrate the basic trend of the $k_{\rm VSC}$ predicted by the current theory. The schematic of the model is provided in Fig. 1, whereas the details are provided in Supporting Information, Sec II. Fig. 3 presents the numerical results of using Eq. 17 (or Eq. 19) to estimate VSC-enhanced experiments. Note that for fully coherent FGR (Eq. 17), one expects to see the collective effect. With incoherent FGR (Eq. 15), one will need a much larger $g_{\rm c}$ for a significant modification of $k_{\rm VSC}$. Nevertheless, the basic trend of the resonance behavior (Fig. 3a), the scaling with the light-matter coupling (Fig. 3b) in terms of $\Omega_{\rm R}$, and the cavity lifetime dependence (Fig. 3c) remains the same. Details of the discussions for these results are provided in Supporting Information, Sec. VII.

Fig. 3a presents the $k_{\rm VSC}$ by changing $\omega_{\rm c}$ using Eq. 17. The result obtained from Eq. 19 is nearly identical to Eq. 17 due to the low cavity lifetime $\tau_{\rm c}=100$ fs. Fig. 3a further shows the sharp resonance behavior of the VSC-modified rate profile at $\omega_{\rm c}=\omega_0=1190\ {\rm cm}^{-1}$. Similar sharp resonance has been observed in the VSC experiments[1,5,6] and the quantum dynamics simulations.[39] The similarity of the optical profile of the vibrational absorption and the cavity-modified rate constant observed in the experiments[1] strongly suggests that both have a common origin that corresponds to the $|\nu_{\rm L}\rangle\rightarrow|\nu_{\rm L}'\rangle$ transition. For the optical absorption spectra, the transition is caused by $-\hat{\mu}\cdot E(t)$, where $\hat{\mu}$ is the transition dipole operator, and $E(t)$ is the classical laser field. For the VSC-modified rate profile, the same transition is caused by the molecule-cavity coupling $\hat{\mu}\otimes\sum_{\mathbf{k}}(\hat{a}_{\mathbf{k}}^\dagger+\hat{a}_{\mathbf{k}})\propto\hat{\mu}\otimes\hat{q}_{\mathbf{k}}$, where the thermal fluctuation of the cavity field promotes the transition. The key component for this correct description is to have the quantum frequency ω_0 between $|\nu_{\rm L}\rangle$ state and $|\nu_{\rm L}'\rangle$ state, which are obtained by solving the Schrödinger Equation of the molecular potential. Any rate theories that do not have the vibrational eigenstate information[22,34,41] are less likely to correctly describe such a sharp resonance behavior.

Fig. 3b highlights the quadratic dependence of $k/k_0\propto\Omega_{\rm R}^2$, where $k_0=2.3\times10^{-6}$ fs^{-1} was taken from the exact simulation for the same model.[39] This quadratic behavior of k/k_0 with respect to $\Omega_{\rm R}$ originates from the FGR. Although lack of detailed experimental verification, existing experimental results[1,5] do show a *non-linear* change of the rate constant with respect to $\Omega_{\rm R}$ (for example, Fig. 4b in Ref. 5 and Fig. 3a in Ref. 1). Note that the classical VSC theories[31,39] predict that the rate constant enhancement scales linearly with $\Omega_{\rm R}$ (or scales with $\sqrt{N}$) due to the classical mechanism of the energy redistribution[31] among molecules mediated by the cavity mode. The coherent version of the quantum transition state theory,[57] on the other hand, predicts that k/k_0 scales with $\Omega_{\rm R}^2$. As such, future experimental studies that focus on investigating the basic scaling between k/k_0 and $\Omega_{\rm R}$ will help to verify/rule out certain theories.

This change of rate constant (red curve) in Fig. 3b can also be interpreted as an effective bar-

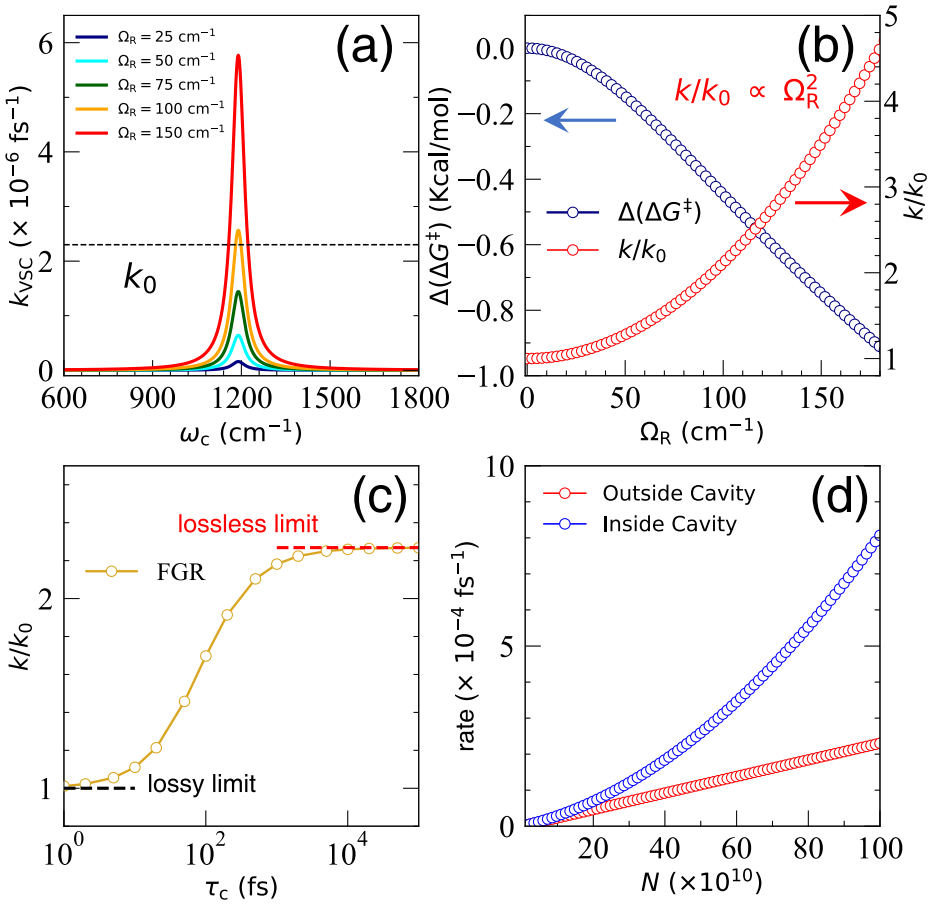

Figure 3: Numerical evaluation of the $k_{\rm VSC}$ in Eq. 17. (a) The profile of the resonant VSC rate constant $k_{\rm VSC}$ as a function of ω_c with different Ω_R (Eq. 6). The cavity lifetime is set to $\tau_c = 100$ fs. (b) The VSC modification k/k_0 (red) as a function of Ω_R at the resonance condition $\omega_c = \omega_0$. The effective change of the free energy barrier $\Delta(\Delta G^{\ddagger})$ (blue) is also plotted. (c) Rate constant modification $k/k_0 = 1 + \tilde{k}_{\rm VSC}/k_0$ as a function of τ_c, where $\tilde{k}_{\rm VSC}$ is evaluated using Eq. 19. (d) Reaction rate $\mathcal{R}$ (Eq. 22) as a function of N for outside the cavity (red) and inside the cavity case (blue) for the fully coherent FGR picture.

rier height change[1,5] as $\Delta(\Delta G^{\ddagger}) \equiv -k_B T \ln(k/k_0)$ (see blue curve in Fig. 3b), if one chooses to interpret the VSC effect from transition state theory.[1,4,5] Of course, using transition state theory is not an appropriate interpretation because the light-matter interaction does not directly modify the barrier.[19,21,22] These observed $\Delta(\Delta G^{\ddagger})$ values should be interpreted as pure kinetics effects.[22] Nevertheless, from the numerical result of Fig. 3b, it is clear that an $\Omega_R = 150$ cm^{-1} can cause a $\Delta(\Delta G^{\ddagger}) \approx 0.8$ Kcal/mol (or 3.3 KJ/mol), explaining the similar basic experimental trend observed in several VSC experiments.[11] It is also clear why $\Delta(\Delta G^{\ddagger})$ has to be non-linearly related[19] to Ω_R, due to the FGR nature of the rate constant modification.

Fig. 3c presents the $k_{\rm VSC}$ when $\omega_c = \omega_0$ as a function of cavity lifetime τ_c (on a log scale in τ_c). The rate constant modification changes in a sigmoid trend. To the best of our knowledge, there is no direct experimental verification of this trend. Note that the current prediction is opposite compared to those in Ref. 39, which suggests an enhanced VSC effect (an increase of rate constant) when decreasing the cavity lifetime τ_c. It must be noted that our approach to modifying cavity loss is different than what was done in Ref. 39. In Ref. 39, the coupling parameter between the cavity mode and far-field modes are scaled to increase cavity loss, while keeping the coupling between cavity mode and molecule as a constant. Therefore, the total reorganization energy of the total effective spectral density is increased with increasing cavity loss. In this work, the cavity lifetime is described as a broadening parameter in the effective spectral density $J_{\rm eff}(\omega)$ (see Supporting Information, Sec. IV), which keeps the total effective reorganization energy of the cavity mode and its bath the same while varying τ_c. This

is likely the reason why our results differ from those of Ref. 39. We should also emphasize that both descriptions might be experimentally relevant and are subject to experimental verification.

Fig. 3d presents the reaction rate $\mathcal{R}$ under the coherent FGR theory (Eq. 22) as a function of N (using Eq. 22), under a coupling strength g_c for $\Omega_R = 150$ cm^{-1} when $N = 10^{12}$. As one expected, outside the cavity, $R = Nk_0$ and scales linearly with N. Inside the cavity, when the rate constant is dominated by k_{VSC}, $\mathcal{R}$ starts to show N^2 scaling. This trend closely resembles the recent experimental observations, for example, Fig. 4b in Ref. 10. Future experiments are needed to confirm this non-linear trend. On the other hand, let us emphasize that this prediction of $\mathcal{R}$ is only true if we consider the fully aligned dipole in the coherent picture (Eq. 17), and disappears when considering the isotropic dipoles or the incoherent FGR theory (Eq. 15).

Suppression Effect. Although we have not discussed the VSC-suppressed reactivities, the cavity-suppressed steady-state population and the rate constant k_1 have been observed in classical[22–24,27,56] and quantum simulations,[8,40] when the molecular system is originally under the high friction limit (after Kramers turnover,[49,50] or so-called spatial diffusion-limited regime). As such, if we treat k_{VSC} as a back-reaction rate constant (associated with the $\{|\nu_L'^j\rangle\} \to |G\rangle$ transition) and take the steady state approximation, the rate constant can be expressed as $k = k_0/(1 + k_{VSC}/k_0)$. Future work is needed to fully investigate this scenario.

Summary and Key Predictions. We present a quantum mechanical theory to explain the current VSC experiments, including the origin of the resonance condition at the norm incident direction (Eq. 16). To the best of our knowledge, this is the *first theory* that successfully explains such an effect. Further assuming the coherent picture of FGR, one can also observe the collective effect of VSC, if all the dipoles are fully aligned. On the other hand, if we assume incoherent FGR, or having isotropically distributed dipoles, then the current theory can not explain the observed collective effect and only when a few molecules are strongly coupled to the cavity can the current theory predict the cavity modifications to the rate constant. This is the limitation of the current theory and future work is needed to fully address these issues.

The current theory predicts the following features of the VSC-modified chemical kinetics.

(1) Under the resonance condition $\omega_c = \omega_0$ (where $k_\parallel = 0$), the rate constant change $k/k_0 = 1 + k_{VSC}/k_0$ will scale as $k/k_0 \propto 1 + \mathcal{C} \cdot (\Omega_R/2\omega_0)^2$, where $\mathcal{C}$ is a constant. The *effective* free energy barrier modification scales as $\Delta(\Delta G^\ddagger) \propto -k_B T \ln\left[1 + \mathcal{C} \cdot (\Omega_R/2\omega_0)^2\right]$, which is a non-linear function[1,5] of Ω_R.

(2) The VSC modification will increase with cavity lifetime τ_c, and diminish to zero as $\tau_c \to 0$.

(3) The VSC-enhanced effect will saturate with an increasing Ω_R, such that $k_1 \gg k_2, k_3$ breaks the mechanistic hypothesis.

(4) For two chemically similar reactions, if one satisfies $k_1 \ll k_2, k_3$ but the other does not, then the current theory predicts that there will be VSC effect for the first reaction but not for the second one.

Supporting Information. The Supporting Information is available free of charge at [url]. A detailed derivation of the Hamiltonian; details of the molecular system, including the table of major parameters; analysis of the Rabi splitting; the effective Hamiltonian and effective spectral density derived by applying harmonic analysis to classical equations of motion; density of states analysis for the Fabry-Pérot cavity; derivation of the VSC-modified rate constant expression in Eq. 19-20 of the main text; details about the numerical results in Fig. 3.

Acknowledgement. This work was supported by the National Science Foundation Award under Grant No. CHE-2244683. P.H. appreciates the support of the Cottrell Scholar Award (a program by the Research Corporation for Science Advancement). M.A.D.T. appreciates the support from the National Science Foundation Graduate Research Fellowship Program under Grant No. DGE-1939268. We appreciate valuable discussions with Jino George, Tao Li, Eric Koessler, and Arkajit Mandal.

References

(1) Thomas, A.; George, J.; Shalabney, A.; Dryzhakov, M.; Varma, S. J.; Moran, J.; Chervy, T.; Zhong, X.; Devaux, E.; Genet, C.; Hutchison, J. A.; Ebbesen, T. W. Ground-State Chemical Reactivity under Vibrational Coupling to the Vacuum Electromagnetic Field. *Angew. Chem. Int. Ed.* **2016**, *55*, 11462–11466.

(2) Vergauwe, R. M. A.; Thomas, A.; Nagarajan, K.; Shalabney, A.; George, J.; Chervy, T.; Seidel, M.;

Devaux, E.; Torbeev, V.; Ebbesen, T. W. Modification of Enzyme Activity by Vibrational Strong Coupling of Water. *Angew. Chem. Int. Ed.* **2019**, *58*, 15324–15328.

(3) Thomas, A.; Lethuillier-Karl, L.; Nagarajan, K.; Vergauwe, R. M. A.; George, J.; Chervy, T.; Shalabney, A.; Devaux, E.; Genet, C.; Moran, J.; Ebbesen, T. W. Tilting a ground-state reactivity landscape by vibrational strong coupling. *Science* **2019**, *363*, 615–619.

(4) Thomas, A.; Jayachandran, A.; Lethuillier-Karl, L.; Vergauwe, R. M.; Nagarajan, K.; Devaux, E.; Genet, C.; Moran, J.; Ebbesen, T. W. Ground state chemistry under vibrational strong coupling: dependence of thermodynamic parameters on the Rabi splitting energy. *Nanophotonics* **2020**, *9*, 249–255.

(5) Lather, J.; Bhatt, P.; Thomas, A.; Ebbesen, T. W.; George, J. Cavity Catalysis by Cooperative Vibrational Strong Coupling of Reactant and Solvent Molecules. *Angew. Chem. Int. Ed.* **2019**, *58*, 10635–10638.

(6) Lather, J.; Thabassum, A. N. K.; Singh, J.; George, J. Cavity catalysis: modifying linear free-energy relationship under cooperative vibrational strong coupling. *Chem. Sci.* **2022**, *13*, 195–202.

(7) Hirai, K.; Takeda, R.; Hutchison, J. A.; Uji-i, H. Modulation of Prins Cyclization by Vibrational Strong Coupling. *Angew. Chem. Int. Ed.* **2020**, *59*, 5332–5335.

(8) Ahn, W.; Triana, J. F.; Recabal, F.; Herrera, F.; Simpkins, B. S. Modification of ground state chemical reactivity via light-matter coherence in infrared cavities. *ChemRxiv* **2023**, *11*, 10.26434/chemrxiv–2022–wb6vs–v2.

(9) Gu, K.; Si, Q.; Li, N.; Gao, F.; Wang, L.; Zhang, F. Regulation of Recombinase Polymerase Amplification by Vibrational Strong Coupling of Water. *ACS Photonics* **2023**, doi.org/10.1021/acsphotonics.3c00243.

(10) Lather, J.; George, J. Improving Enzyme Catalytic Efficiency by Co-operative Vibrational Strong Coupling of Water. *J. Phys. Chem. Lett.* **2021**, *12*, 379–384.

(11) Hirai, K.; Hutchison, J. A.; Uji-i, H. Recent Progress in Vibropolaritonic Chemistry. *ChemPlusChem* **2020**, *85*, 1981–1988.

(12) Nagarajan, K.; Thomas, A.; Ebbesen, T. W. Chemistry under Vibrational Strong Coupling. *J. Am. Chem. Soc.* **2021**, *143*, 16877–16889.

(13) Simpkins, B. S.; Dunkelberger, A. D.; Vurgaftman, I. Control, Modulation, and Analytical Descriptions of Vibrational Strong Coupling. *Chem. Rev.* **2023**, *123*, 5020–5048.

(14) Campos-Gonzalez-Angulo, J. A.; Poh, Y. R.; Du, M.; Yuen-Zhou, J. Swinging between shine and shadow: Theoretical advances on thermally-activated vibropolaritonic chemistry (a perspective). *arXiv* **2023**, 2212.04017.

(15) Galego, J.; Climent, C.; Garcia-Vidal, F. J.; Feist, J. Cavity Casimir-Polder Forces and Their Effects in Ground-State Chemical Reactivity. *Phys. Rev. X* **2019**, *9*, 021057.

(16) Campos-Gonzalez-Angulo, J. A.; Ribeiro, R. F.; Yuen-Zhou, J. Resonant catalysis of thermally activated chemical reactions with vibrational polaritons. *Nat. Commun.* **2019**, *10*, 4685.

(17) Semenov, A.; Nitzan, A. Electron transfer in confined electromagnetic fields. *J. Chem. Phys.* **2019**, *150*, 174122.

(18) Vurgaftman, I.; Simpkins, B. S.; Dunkelberger, A. D.; Owrutsky, J. C. Negligible Effect of Vibrational Polaritons on Chemical Reaction Rates via the Density of States Pathway. *J. Phys. Chem. Lett.* **2020**, *11*, 3557–3562.

(19) Li, T. E.; Nitzan, A.; Subotnik, J. E. On the origin of ground-state vacuum-field catalysis: Equilibrium consideration. *J. Chem. Phys.* **2020**, *152*, 234107.

(20) Zhdanov, V. P. Vacuum field in a cavity, light-mediated vibrational coupling, and chemical reactivity. *Chem. Phys.* **2020**, *535*, 110767.

(21) Campos-Gonzalez-Angulo, J. A.; Yuen-Zhou, J. Polaritonic normal modes in transition state theory. *J. Chem. Phys.* **2020**, *152*, 161101.

(22) Li, X.; Mandal, A.; Huo, P. Cavity frequency-dependent theory for vibrational polariton chemistry. *Nat. Commun.* **2021**, *12*, 1315.

(23) Schäfer, C.; Flick, J.; Ronca, E.; Narang, P.; Rubio, A. Shining Light on the Microscopic Resonant Mechanism Responsible for Cavity-Mediated Chemical Reactivity. *Nat. Commun.* **2022**, *13*, 7817.

(24) Li, X.; Mandal, A.; Huo, P. Theory of Mode-Selective Chemistry through Polaritonic Vibrational Strong Coupling. *J. Phys. Chem. Lett.* **2021**, *12*, 6974–6982.

(25) Li, T. E.; Nitzan, A.; Subotnik, J. E. Collective Vibrational Strong Coupling Effects on Molecular Vibrational Relaxation and Energy Transfer: Numerical Insights via Cavity Molecular Dynamics Simulations. *Angew. Chem. Int. Ed.* **2021**, *60*, 15533–15540.

(26) Li, T. E.; Nitzan, A.; Subotnik, J. E. Polariton relaxation under vibrational strong coupling: Comparing cavity molecular dynamics simulations against Fermi's golden rule rate. *J. Chem. Phys.* **2022**, *156*, 134106.

(27) Mandal, A.; Li, X.; Huo, P. Theory of vibrational polariton chemistry in the collective coupling regime. *J. Chem. Phys.* **2022**, *156*, 014101.

(28) Du, M.; Yuen-Zhou, J. Catalysis by Dark States in Vibropolaritonic Chemistry. *Phys. Rev. Lett.* **2022**, *128*, 096001.

(29) Philbin, J. P.; Wang, Y.; Narang, P.; Dou, W. Chemical Reactions in Imperfect Cavities: Enhancement, Suppression, and Resonance. *J. Phys. Chem. C* **2022**, *126*, 14908–14913.

(30) Wang, D. S.; Neuman, T.; Yelin, S. F.; Flick, J. Cavity-Modified Unimolecular Dissociation Reactions via Intramolecular Vibrational Energy Redistribution. *J. Phys. Chem. Lett.* **2022**, *13*, 3317–3324.

(31) Wang, D. S.; Flick, J.; Yelin, S. F. Chemical reactivity under collective vibrational strong coupling. *J. Chem. Phys.* **2022**, *157*, 224304.

(32) Sun, J.; Vendrell, O. Suppression and Enhancement of Thermal Chemical Rates in a Cavity. *J. Phys. Chem. Lett.* **2022**, *13*, 4441–4446.

(33) Fischer, E. W.; Anders, J.; Saalfrank, P. Cavity-altered thermal isomerization rates and dynamical resonant localization in vibro-polaritonic chemistry. *J. Chem. Phys.* **2022**, *156*, 154305.

(34) Lindoy, L. P.; Mandal, A.; Reichman, D. R. Resonant Cavity Modification of Ground-State Chemical Kinetics. *J. Phys. Chem. Lett.* **2022**, *13*, 6580–6586.

(35) Mondal, S.; Wang, D. S.; Keshavamurthy, S. Dissociation dynamics of a diatomic molecule in an optical cavity. *J. Chem. Phys.* **2022**, *157*, 244109.

(36) Cao, J. Generalized Resonance Energy Transfer Theory: Applications to Vibrational Energy Flow in Optical Cavities. *J. Phys. Chem. Lett.* **2022**, *13*, 10943–10951.

(37) Kansanen, K. S. U.; Heikkilä, T. T. Cavity-induced bifurcation in classical rate theory. *arXiv* **2023**, 2202.12182v3.

(38) Du, M.; Poh, Y. R.; Yuen-Zhou, J. Vibropolaritonic Reaction Rates in the Collective Strong Coupling Regime: Pollak–Grabert–Hänggi Theory. *J. Phys. Chem. C.* **2023**, *127*, 5230–5237.

(39) Lindoy, L. P.; Mandal, A.; Reichman, D. R. Quantum dynamical effects of vibrational strong coupling in chemical reactivity. *Nat. Commun.* **2023**, *14*, 2733.

(40) Anderson, M. C.; Woods, E. J.; Fay, T. P.; Wales, D. J.; Limmer, D. T. On the mechanism of polaritonic rate suppression from quantum transition paths. *arXiv* **2023**, 2304.13024.

(41) Fiechter, M. R.; Runeson, J. E.; Lawrence, J. E.; Richardson, J. O. How Quantum is the Resonance Behavior in Vibrational Polariton Chemistry? 2023.

(42) Wang, D. S.; Yelin, S. F. A Roadmap Toward the Theory of Vibrational Polariton Chemistry. *ACS Photonics* **2021**, *8*, 2818–2826.

(43) Sidler, D.; Ruggenthaler, M.; Schäfer, C.; Ronca, E.; Rubio, A. A perspective on ab initio modeling of polaritonic chemistry: The role of non-equilibrium effects and quantum collectivity. *J. Chem. Phys.* **2022**, *156*, 230901.

(44) Mandal, A.; Taylor, M.; Weight, B.; Koessler, E.; Li, X.; Huo, P. Theoretical Advances in Polariton Chemistry and Molecular Cavity Quantum Electrodynamics. *ChemRxiv* **2022**,

(45) Hopfield, J. J. Theory of the Contribution of Excitons to the Complex Dielectric Constant of Crystals. *Phys. Rev.* **1958**, *112*, 1555–1567.

(46) Tavis, M.; Cummings, F. Exact Solution for an N-Molecule-Radiation-Field Hamiltonian. *Phys. Rev.* **1968**, *170*, 379–384.

(47) Jaynes, E.; Cummings, F. Comparison of Quantum and Semiclassical Radiation Theories with Application to the Beam Maser. *Proc. IEEE* **1963**, *18*, 89–109.

(48) del Pino, J.; Feist, J.; Garcia-Vidal, F. J. Quantum theory of collective strong coupling of molecular vibrations with a microcavity mode. *New J. Phys.* **2015**, *17*, 053040.

(49) Hänggi, P.; Talkner, P.; Borkovec, M. Reaction-rate theory: fifty years after Kramers. *Rev. Mod. Phys.* **1990**, *62*, 251–341.

(50) Pollak, E.; Grabert, H.; Hänggi, P. Theory of Activated Rate Processes for Arbitrary Frequency Dependent Friction: Solution of the Turnover Problem. *J. Chem. Phys.* **1989**, *91*, 4073–4087.

(51) Leggett, A. J. Quantum tunneling in the presence of an arbitrary linear dissipation mechanism. *Phys. Rev. B* **1984**, *30*, 1208–1218.

(52) Garg, A.; Onuchic, J. N.; Ambegaokar, V. Effect of friction on electron transfer in biomolecules. *J. Chem. Phys.* **1985**, *83*, 4491–4503.

(53) Thoss, M.; Wang, H.; Miller, W. H. Self-consistent hybrid approach for complex systems: Application to the spin-boson model with Debye spectral density. *J. Chem. Phys.* **2001**, *115*, 2991–3005.

(54) Hove, L. V. The Occurrence of Singularities in the Elastic Frequency Distribution of a Crystal. *Phys. Rev.* **1953**, *89*, 1189–1193.

(55) Castellanos, M. A.; Huo, P. Enhancing Singlet Fission Dynamics by Suppressing Destructive Interference between Charge-Transfer Pathways. *J. Phys. Chem. Lett.* **2017**, *8*, 2480–2488.

(56) Philbin, J. P.; Haugland, T. S.; Ghosh, T. K.; Ronca, E.; Chen, M.; Narang, P.; Koch, H. Molecular van der Waals fluids in cavity quantum electrodynamics. 2022.

(57) Yang, P.-Y.; Cao, J. Quantum Effects in Chemical Reactions under Polaritonic Vibrational Strong Coupling. *J. Phys. Chem. Lett.* **2021**, *12*, 9531–9538.

Supporting Information:

Resonance Theory of Vibrational Polariton Chemistry

Wenxiang Ying,[†] Michael A.D. Taylor,[‡] and Pengfei Huo[*,†,‡]

†*Department of Chemistry, University of Rochester, 120 Trustee Road, Rochester, New York 14627, USA*

‡*Institute of Optics, Hajim School of Engineering, University of Rochester, Rochester, New York, 14627, USA*

E-mail: pengfei.huo@rochester.edu

I. Details of the Hamiltonian

We start with the Pauli-Fierz Hamiltonian of many molecules coupled to many modes under the dipole approximation. This Hamiltonian is obtained by performing the Power-Zienau-Woolley (PZW) gauge transformation[1–3] on the minimum coupling Hamiltonian. The details can be found in Ref. 4 (Sec. 2.6) or Ref. 5 (Chapter 2.2). The Hamiltonian is then further projected on the ground electronic states of all molecules.

The total Hamiltonian is expressed as

$$\hat{H} = \hat{H}_{\rm M} + \hat{H}_{\rm ph} + \hat{H}_{\rm loss} \tag{S1}$$
$$+ \sum_{\mathbf{k}} \Big[\sqrt{\frac{\hbar\omega_{\mathbf{k}}}{2}} \lambda_{\rm c} \sum_j (\hat{a}^\dagger_{\mathbf{k}} e^{-i\mathbf{k}\cdot\bar{\boldsymbol{x}}_j} + \hat{a}_{\mathbf{k}} e^{i\mathbf{k}\cdot\bar{\boldsymbol{x}}_j})(\hat{\mathrm{e}}_{\mathbf{k}} \cdot \hat{\boldsymbol{\mu}}_j(\hat{\mathbf{R}}_j)) + \frac{\lambda_{\rm c}^2}{2} \sum_{i,j} (\hat{\mathrm{e}}_{\mathbf{k}} \cdot \hat{\boldsymbol{\mu}}_i(\hat{\mathbf{R}}_i))(\hat{\mathrm{e}}_{\mathbf{k}} \cdot \hat{\boldsymbol{\mu}}_j(\hat{\mathbf{R}}_j)) e^{-i\mathbf{k}\cdot(\bar{\boldsymbol{x}}_i - \bar{\boldsymbol{x}}_j)} \Big],$$

where the $\{i, j\}$ iterates over the molecules in the cavity, $\bar{\boldsymbol{x}}_j$ is the center of mass of the $j_{\rm th}$ molecule, $\hat{H}_{\rm M}$ is the bare matter Hamiltonian, $\hat{H}_{\rm ph}$ is the pure photonic Hamiltonian. Further, $\hat{H}_{\rm M}$ is the molecular Hamiltonian

$$\hat{H}_{\rm M} = \sum_{j=1}^{N} \Big(\frac{\hat{P}_j^2}{2M} + V(\hat{R}_j) \Big) + \hat{H}_\nu, \tag{S2}$$

where $\hat{R}_j$ is the reaction coordinate for the j_{th} molecule, $V(\hat{R})$ is the ground state potential for all reaction molecules (typically double well potential), and $\mu(\hat{R}_j)$ is the dipole associated with the ground electronic state (electronic permanent dipole). In this work, we have explicitly ignored the interactions among molecules and treated them as independent, identical molecules. We further introduce the effects of a phonon bath to the Hamiltonian via a system-bath term, which reads as

$$\hat{H}_\nu = \frac{1}{2}\sum_j \sum_\zeta \Big[\hat{p}_{j,\zeta}^2 + \omega_{j,\zeta}^2\Big(\hat{x}_{j,\zeta} - \frac{c_{j,\zeta}}{\omega_{j,\zeta}^2}\hat{R}_j\Big)^2\Big], \tag{S3}$$

where $\{\hat{x}_{j,\zeta},\ \hat{p}_{j,\zeta}\}$ are the mass-weighted coordinate and momentum pair of the $\{j,\zeta\}$-th bath oscillator that directly couples to the reaction coordinate of molecule j. The j-th phonon bath as well as its coupling to the reaction coordinate R_j can be described by the spectral density function[6]

$$J_\nu(\omega) = \frac{\pi}{2}\sum_j \sum_\zeta \frac{c_{j,\zeta}^2}{\omega_{j,\zeta}}\delta(\omega - \omega_{j,\zeta}), \tag{S4}$$

where $\omega_{j,\zeta}$, $c_{j,\zeta}$ are the oscillator frequencies and coupling coefficients, respectively. Note that we have assumed an identical spectral density for all molecule $j \in [1, N]$.

By introducing the photon mode coordinate and momentum operators

$$\hat{q}_{\mathbf{k}} = \sqrt{\hbar/2\omega_{\mathbf{k}}}(\hat{a}_{\mathbf{k}}^\dagger + \hat{a}_{\mathbf{k}}), \qquad \hat{p}_{\mathbf{k}} = i\sqrt{\hbar\omega_{\mathbf{k}}/2}(\hat{a}_{\mathbf{k}}^\dagger - \hat{a}_{\mathbf{k}}), \tag{S5}$$

or inversely, the field operators

$$\hat{a}_{\mathbf{k}} = \sqrt{\frac{\omega_{\mathbf{k}}}{2\hbar}}\hat{q}_{\mathbf{k}} + i\sqrt{\frac{1}{2\hbar\omega_{\mathbf{k}}}}\hat{p}_{\mathbf{k}}, \qquad \hat{a}_{\mathbf{k}}^\dagger = \sqrt{\frac{\omega_{\mathbf{k}}}{2\hbar}}\hat{q}_{\mathbf{k}} - i\sqrt{\frac{1}{2\hbar\omega_{\mathbf{k}}}}\hat{p}_{\mathbf{k}}, \tag{S6}$$

Eq. S1 can be alternatively expressed as

$$\hat{H} = \hat{H}_{\text{M}} + \frac{1}{2}\sum_{\mathbf{k}}\Big[(\hat{p}_{\mathbf{k}} - \lambda_{\text{c}}\hat{\Pi}_{\mathbf{k}})^2 + (\omega_{\mathbf{k}}\hat{q}_{\mathbf{k}} + \lambda_{\text{c}}\hat{\mathcal{S}}_{\mathbf{k}})^2\Big] + \hat{H}_{\text{loss}}, \tag{S7}$$

where the collective system operators are defined as

$$\hat{\Pi}_{\mathbf{k}} = \sum_j (\hat{\mathrm{e}}_{\mathbf{k}} \cdot \hat{\boldsymbol{\mu}}_j(\hat{\mathbf{R}}_j)) \sin(\mathbf{k} \cdot \bar{\boldsymbol{x}}_j), \tag{S8a}$$

$$\hat{\mathcal{S}}_{\mathbf{k}} = \sum_j (\hat{\mathrm{e}}_{\mathbf{k}} \cdot \hat{\boldsymbol{\mu}}_j(\hat{\mathbf{R}}_j)) \cos(\mathbf{k} \cdot \bar{\boldsymbol{x}}_j). \tag{S8b}$$

To account for cavity loss, we further introduce the photon-loss Hamiltonian which is also based on the system-bath model, defined as

$$\hat{H}_{\mathrm{loss}} = \frac{1}{2} \sum_{\mathbf{k},\zeta} \Big[\hat{p}^2_{\mathbf{k},\zeta} + \omega^2_{\mathbf{k},\zeta} \Big(\hat{x}_{\mathbf{k},\zeta} - \frac{c_{\mathbf{k},\zeta}}{\omega^2_{\mathbf{k},\zeta}} \hat{q}_{\mathbf{k}} \Big)^2 \Big], \tag{S9}$$

where $\{\hat{x}_{\mathbf{k},\zeta}, \hat{p}_{\mathbf{k},\zeta}\}$ are the mass-weighted coordinate and momentum operators of the $\{\mathbf{k},\zeta\}$-th non-cavity bath mode, respectively, which directly couple to the photon mode coordinate operator $\hat{q}_{\mathbf{k}}$. The $\mathbf{k}$-th photon-loss bath as well as its coupling to the photon mode coordinate operator $\hat{q}_{\mathbf{k}}$ are described by the spectral density function

$$J_{\mathrm{loss}}(\omega, \mathbf{k}) = \frac{\pi}{2} \sum_{\zeta} \frac{c^2_{\mathbf{k},\zeta}}{\omega_{\mathbf{k},\zeta}} \delta(\omega - \omega_{\mathbf{k},\zeta}), \tag{S10}$$

where $\omega_{\mathbf{k},\zeta}$, $c_{\mathbf{k},\zeta}$ are the oscillator frequencies and coupling coefficients, respectively.

Based on the above discussions, the collective PF Hamiltonian in Eq. S7 is expressed in the projected subspace as

$$\hat{H} = \sum_j \frac{\hat{P}_j}{2M_j} + E_g(R_j) + \hat{H}_\nu + \frac{1}{2} \sum_{\mathbf{k}} \Big[(\hat{p}_{\mathbf{k}} - \lambda_{\mathrm{c}} \hat{\Pi}_{\mathbf{k}})^2 + (\omega_{\mathbf{k}} \hat{q}_{\mathbf{k}} + \lambda_{\mathrm{c}} \hat{\mathcal{S}}_{\mathbf{k}})^2 \Big] + \hat{H}_{\mathrm{loss}}, \tag{S11}$$

where

$$\hat{\Pi}_{\mathbf{k}} = \sum_j \mu_j(\hat{R}_j) \cdot \cos\varphi_j \cdot \sin(\mathbf{k} \cdot \bar{\boldsymbol{x}}_j), \tag{S12a}$$

$$\hat{\mathcal{S}}_{\mathbf{k}} = \sum_j \mu_j(\hat{R}_j) \cdot \cos\varphi_j \cdot \cos(\mathbf{k} \cdot \bar{\boldsymbol{x}}_j), \tag{S12b}$$

where $\mu_j(\hat{R}_j)$ is the ground state permanent dipole moment of molecule j, and φ_j is the relative

angle between the dipole vector and the field polarization direction $\hat{\mathrm{e}}_{\mathbf{k}}$.

For simplicity, in this work we assume the *long wavelength approximation* where the transverse fields can be treated as spatially uniform, *i.e.*, $e^{i\mathbf{k}\cdot\mathbf{r}} \approx 1$, such that

$$\hat{\mathbf{A}}_\perp(\mathbf{r}) \approx \hat{\mathbf{A}}_\perp = \sum_{\mathbf{k}} \frac{\hat{\mathrm{e}}_{\mathbf{k}}}{\omega_{\mathbf{k}}} \sqrt{\frac{\hbar\omega_{\mathbf{k}}}{2\varepsilon_0 \mathcal{V}}} (\hat{a}_{\mathbf{k}} + \hat{a}_{\mathbf{k}}^\dagger), \tag{S13}$$

which leads to $\cos(\mathbf{k}\cdot\bar{\boldsymbol{x}}_j) = 1$, $\sin(\mathbf{k}\cdot\bar{\boldsymbol{x}}_j) = 0$, $\hat{\Pi}_{\mathbf{k}} = 0$ and $\hat{\mathcal{S}}_{\mathbf{k}} = \sum_j \mu_j(\hat{R}_j)\cdot\cos\varphi_j$. Then the collective PF Hamiltonian of Eq. S11 can be further simplified as

$$\hat{H}_{\mathrm{PF}}^{[N]} = \sum_j \frac{\hat{P}_j}{2M} + V(R_j) + \hat{H}_\nu + \frac{1}{2}\sum_{\mathbf{k}} \Big[\hat{p}_{\mathbf{k}}^2 + \omega_{\mathbf{k}}^2 \Big(\hat{q}_{\mathbf{k}} + \frac{\lambda_{\mathrm{c}}}{\omega_{\mathbf{k}}} \sum_j \mu(\hat{R}_j)\cdot\cos\varphi_j\Big)^2\Big] + \hat{H}_{\mathrm{loss}}, \tag{S14}$$

which is the VSC Hamiltonian in Eq. 1 of the main text. To summarize, we have explicitly assumed that there are no intermolecular interactions, as well as the long wavelength approximation. Their presence might influence the final rate constant expression k_{VSC}, however, they are not playing any dominant role in order to provide a theory as we have shown here to capture resonant effect and collective effect.

II. Details of the Molecular Model System

To model how VSC influences chemical reactions, we are particularly interested in the one-dimensional double-well (DW) potential[7,8]

$$V(\hat{R}) = -\frac{M\omega_{\mathrm{b}}^2}{2}\hat{R}^2 + \frac{M^2\omega_{\mathrm{b}}^4}{16E_{\mathrm{b}}}\hat{R}^4, \tag{S15}$$

where M is the effective mass of the reaction coordinate, ω_{b} is the barrier frequency, and E_{b} is barrier height of the DW potential. Note that Eq. S15 assumes a symmetric DW potential.

For the system (reaction coordinate), the corresponding eigenvectors $|\nu_i\rangle$ and eigenenergies E_i are obtained by numerically solving

$$\Big(\frac{\hat{P}^2}{2M} + V(\hat{R})\Big)|\nu_i\rangle = E_i|\nu_i\rangle, \tag{S16}$$

where $V(\hat{R})$ is expressed in Eq. S15. These vibrational eigenstates are obtained by using the discrete variable representation (DVR) basis.[9] We *diabatize* the two lowest eigenstates as

$$|\nu_{\rm L}\rangle = \frac{1}{\sqrt{2}}\big(|\nu_0\rangle + |\nu_1\rangle\big), \qquad |\nu_{\rm R}\rangle = \frac{1}{\sqrt{2}}\big(|\nu_0\rangle - |\nu_1\rangle\big), \tag{S17}$$

which leads to two energetically degenerate diabatic states, denoted as $|\nu_{\rm L}\rangle$ and $|\nu_{\rm R}\rangle$ for states localized in the left and right wells, respectively, both with the degenerate energy $E_{\rm L} = (E_1 + E_0)/2$ and a small tunneling splitting $V^0_{\rm LR} = (E_1 - E_0)/2$ (where the energy difference between E_1 and E_0 is $2V^0_{\rm LR}$). Similarly, for $\{|\nu_2\rangle, |\nu_3\rangle\}$, one can diabatize them and obtain the first excited *diabatic vibrational state* in the left well and right well as follows

$$|\nu'_{\rm L}\rangle = \frac{1}{\sqrt{2}}\big(|\nu_2\rangle + |\nu_3\rangle\big), \qquad |\nu'_{\rm R}\rangle = \frac{1}{\sqrt{2}}\big(|\nu_2\rangle - |\nu_3\rangle\big), \tag{S18}$$

with the degenerate diabatic energy $E_{\rm L'} = (E_3 + E_2)/2$ and the tunneling splitting $V_{\rm LR} = (E_3 - E_2)/2$. Based on the two diabatic states $|\nu_{\rm L}\rangle$ and $|\nu'_{\rm L}\rangle$ in the left well, we define the quantum vibration frequency of the reactant as

$$\hbar\omega_0 \equiv E_{\rm L'} - E_{\rm L}, \tag{S19}$$

which is directly related to the quantum transition of $|\nu_{\rm L}\rangle \to |\nu'_{\rm L}\rangle$. Note that the spectroscopy measurement (IR or transmission spectra) is also directly related to this frequency.

For a practical calculation, truncation has to be made upon the number of matter states, restricting the dynamics in a relatively low energy subspace while ensuring numerical accuracy. As such, the Hamiltonian and the reaction coordinate have their matrix representations in a truncated Hilbert space. Similarly, we also have the vibrational permanent dipole associated with $|\nu_{\rm L}\rangle$ as $\mu_{\rm LL} = \langle\nu_{\rm L}|\mu(\hat{R})|\nu_{\rm L}\rangle$, as well as for vibrationally excited states $|\nu'_{\rm L}\rangle$ as $\mu_{\rm L'L'} = \langle\nu'_{\rm L}|\mu(\hat{R})|\nu'_{\rm L}\rangle$. These permanent dipoles might be important for computing polariton spectra under ultra-strong coupling regimes. For rate constants, we find that they might be important to provide constant shifts of vibrational states under very large coupling limits. We have ignored them for the simplicity of the theory.

Fig. 1 of the main text provides a schematic illustration of the ground state chemical reaction model (single molecule) and the first few vibrational states of the DW model, denoted as $|\nu_{\rm L}\rangle$, $|\nu_{\rm R}\rangle$, $|\nu'_{\rm L}\rangle$, $|\nu'_{\rm R}\rangle$. The red arrows indicate the potential effect of the cavity modifying vibrational state transitions, and the green arrow right above the barrier denotes to the fast dissipative tunneling process from $|\nu'_{\rm L}\rangle$ to $|\nu'_{\rm R}\rangle$. Here, we use the parameters $E_{\rm b} = 2250$ cm^{-1}, and $\hbar\omega_{\rm b} = 1000$ cm^{-1}.[10] The eigenstates are obtained with the sinc-DVR basis with 1001 grid points in the range of $-100 \leq R \leq 100$, then diabatized according to Eq. S17 and S18. Note that because $|\nu'_{\rm L}\rangle$ and $|\nu'_{\rm R}\rangle$ are very close to the top of the barrier, they are not as well localized as $|\nu_{\rm L}\rangle$ and $|\nu_{\rm R}\rangle$.

To be more clear, we briefly summarize the major parameters for the system degrees of freedom (DOF) in Table 1.[10]

Table 1: Table of major parameters

Parameters of system DOF	Notation	Value
Effective mass of the reaction coordinate	M	1 a.u.
Barrier height	$E_{\rm b}$	2250 cm^{-1}
Barrier frequency	$\hbar\omega_{\rm b}$	1000 cm^{-1}
Vibration frequency (or resonance frequency)	$\hbar\omega_0$	1190 cm^{-1}
Tunneling splitting between $\|\nu_{\rm L}\rangle$ and $\|\nu_{\rm R}\rangle$	$V^0_{\rm LR}$	1.03 cm^{-1}
Tunneling splitting between $\|\nu'_{\rm L}\rangle$ and $\|\nu'_{\rm R}\rangle$	$V_{\rm LR}$	47.68 cm^{-1}

We further show that the subsequent step $\{|\nu'^j_{\rm L}\rangle\} \xrightarrow{k_2} \{|\nu'^j_{\rm R}\rangle\}$ will occur with the same rate constant k_2 as for the cavity free case, such that there is *no additional* change of this step due to coupling to the cavity. Note that outside the cavity, this rate is controlled by the tunneling-splitting coupling between $|\nu'^j_{\rm L}\rangle$ and $|\nu'^j_{\rm R}\rangle$, denoted as $V_{\rm LR} = \langle\nu'^j_{\rm R}|\hat{V}_j|\nu'^j_{\rm L}\rangle$, which is assumed to be identical for all molecules j. The localness of chemical reactions ensures that $\langle\nu'^i_{\rm R}|\hat{V}_j|\nu'^k_{\rm L}\rangle = V_{\rm LR}\delta_{ij}\delta_{jk}$, *i.e.*, the reaction occurs locally. Using similar Fermi's Golden Rule (FGR) argument for the $\{|\nu'^j_{\rm L}\rangle\} \xrightarrow{k_2} \{|\nu'^j_{\rm R}\rangle\}$ transition, We assume that by reaching the steady state populations, all $|\nu'^j_{\rm L}\rangle$ are equally populated, such that each channel should be weighted by $1/N$. Using FGR, and considering a resonant energy tunneling transition between $|\nu'^j_{\rm L}\rangle$ and $|\nu'^j_{\rm R}\rangle$, the tunneling rate constant k_2 is

$$k_2 \propto \frac{1}{N}\sum_{j=1}^{N} |\langle\nu'^j_{\rm R}|\hat{V}_j|\nu'^j_{\rm L}\rangle|^2 \propto V^2_{\rm RL}, \tag{S20}$$

indicating that k_2 is identical to the single molecule tunneling rate outside the cavity. As such, the molecule-cavity interaction will not change the local bond-breaking process.

III. Analysis of the Rabi Splitting

To quickly review the well-known results of Rabi splitting through collective light-matter couplings, let us assume all dipoles are fully aligned, such that $\cos\varphi_j = 1$ for all j. We further introduce the $\sigma_j = |G\rangle\langle\nu_j|$ and $\sigma_j^\dagger = |\nu_i\rangle\langle G|$ as the raising and lowering operators of the molecular vibrational excitation on molecule j. In the single excited subspace $\mathcal{P} = |G\rangle\langle G| + \sum_j |\nu_j\rangle\langle\nu_j|$, the $\mu(\hat{R}_j)$ operator becomes

$$\hat{\mathcal{P}}\mu(\hat{R}_j)\hat{\mathcal{P}} = \mu_{\mathrm{LL}'} \cdot (\sigma_j^\dagger + \sigma_j), \tag{S21}$$

where $\mu_{\mathrm{LL}'} = \langle \nu_{\mathrm{L}}'^j | \mu(\hat{R}_j) | \nu_{\mathrm{L}}^j \rangle$ is identical to all molecules. Here, we explicitly ignored the permanent dipole contributions $\langle \nu_{\mathrm{L}}^j | \hat{R}_j | \nu_{\mathrm{L}}^j \rangle$ and $\langle \nu_{\mathrm{L}}'^j | \hat{R}_j | \nu_{\mathrm{L}}'^j \rangle$, which for our model have very small matrix elements. They could be important for computing the polariton eigenspectrum when the coupling strength λ_{c} is very large.

Using the above notations, one can rewrite the light-matter coupling term as

$$\hat{H}_{\mathrm{LM}}^{[N]} = \hbar g_{\mathrm{c}} \sqrt{\omega_{\mathbf{k}}} \cdot \sum_j \sum_{\mathbf{k}} (\hat{\sigma}_j + \hat{\sigma}_j^\dagger)(\hat{a}_{\mathbf{k}} + \hat{a}_{\mathbf{k}}^\dagger), \tag{S22}$$

where $g_{\mathrm{c}} = \mu_{\mathrm{LL}'}\lambda_{\mathrm{c}}/\sqrt{2}\hbar$. When assuming $\cos\varphi_j = 1$, Eq. S14 will have permutation symmetry, and one can introduce the collective operators

$$\hat{\sigma}_N^\dagger = \frac{1}{\sqrt{N}} \sum_j |\nu_j\rangle\langle G|, \quad \hat{\sigma}_N = \frac{1}{\sqrt{N}} \sum_j |G\rangle\langle\nu_j|. \tag{S23}$$

Using the collective operators, and ignoring the counter-rotating wave term ($\propto \sum_{j,\mathbf{k}} (\hat{\sigma}_j^\dagger \hat{a}_{\mathbf{k}}^\dagger + \hat{\sigma}_j \hat{a}_{\mathbf{k}})$), which is less important for the resonant condition of $\omega_{\mathbf{k}} = \omega_0$ when g_{c} is small, we have

$$\hat{H}_{\mathrm{LM}}^{[N]} = \sqrt{N}\hbar g_{\mathrm{c}} \sqrt{\omega_{\mathbf{k}}} \cdot \sum_{\mathrm{k}} (\sigma_N^\dagger \hat{a}_{\mathbf{k}} + \sigma_N \hat{a}_{\mathbf{k}}^\dagger). \tag{S24}$$

This level of approximation is commonly referred to as the Holstein-Tavis-Cummings model. Note

that the effective coupling between light and matter is now $\sqrt{N}g_{\rm c}$. This light-matter coupling term will hybridize the 1 photon-dressed ground state $|G\rangle \otimes |1_{\mathbf{k}}\rangle$ with the 0-photon dressed bright state $|B\rangle \otimes |0_{\mathbf{k}}\rangle$, generating the following polariton states

$$|+\rangle = \cos\phi_N \cdot |\mathrm{B}\rangle \otimes |0_{\mathbf{k}}\rangle + \sin\phi_N \cdot |G\rangle \otimes |1_{\mathbf{k}}\rangle, \tag{S25a}$$

$$|-\rangle = -\sin\phi_N \cdot |\mathrm{B}\rangle \otimes |0_{\mathbf{k}}\rangle + \cos\phi_N \cdot |G\rangle \otimes |1_{\mathbf{k}}\rangle, \tag{S25b}$$

where the mixing angle, ϕ_N, is defined as

$$\phi_N = \frac{1}{2}\tan^{-1}[(2\sqrt{N\omega_{\mathbf{k}}}g_{\rm c})/(\omega_{\mathbf{k}}(k_{\|}) - \omega_0)], \tag{S26}$$

with the maximum mixing between light and matter occuring when $\omega_{\rm c}(\mathbf{k}) = \omega_0$. The dark states, on the other hand, do not mix with the photonic DOF under this approximation and remain to be $|\mathrm{D}_\alpha\rangle \otimes |0_{\mathbf{k}}\rangle$ in the singly excited subspace. It is a well-known fact that $\langle G| \otimes \langle 1_{\mathbf{k}}|\hat{H}_{\rm LM}|\mathrm{D}_\alpha\rangle \otimes |0_{\mathbf{k}}\rangle = 0$, because $\langle G|\sum_j(\sigma_j + \sigma_j^\dagger)|\sum_k \mathcal{C}_k^\alpha|\nu_k\rangle = \sum_j\langle\nu_j|\sum_k \mathcal{C}_k^\alpha|\nu_k\rangle = \sum_k \mathcal{C}_k^\alpha = 0$. The energy gap between the upper polariton state and the lower polariton state is referred to as the Rabi splitting and is expressed as follows

$$\Omega_{\rm R} \equiv E_+ - E_- = \sqrt{(\omega_{\mathbf{k}} - \omega_0)^2 + 4N\omega_{\rm c}g_{\rm c}^2}, \tag{S27}$$

and under the resonant condition $\omega_{\mathbf{k}} = \omega_0$, the Rabi splitting is $\Omega_R = 2\sqrt{N\omega_{\rm c}}g_{\rm c} = \sqrt{\frac{2\omega_{\mathbf{k}}}{\epsilon_0\hbar}}\sqrt{\frac{N}{\mathcal{V}}} \cdot \mu_{\mathrm{LL}'}$. As one can clearly see, forming the Rabi splitting is originated from a collective phenomenon, resulting in the well know $\sqrt{N}$ dependence or $\sqrt{N/\mathcal{V}}$ dependence (square root of concentration), confirmed by experiments.[11]

The dark states, on the other hand, do not mix with the photonic DOF under this simplified approximation and remain to be $|\mathrm{D}_\alpha\rangle \otimes |0_{\mathbf{k}}\rangle$ in the single excited subspace. This is because $\langle G| \otimes \langle 1_{\mathbf{k}}|\hat{H}_{\rm LM}|\mathrm{D}_\alpha\rangle \otimes |0_{\mathbf{k}}\rangle = 0$, due to the fact that $\langle G|\sum_j(\sigma_j + \sigma_j^\dagger)|\sum_k \mathcal{C}_k^\alpha|\nu_k\rangle = \sum_j\langle\nu_j|\sum_k \mathcal{C}_k^\alpha|\nu_k\rangle = \sum_k \mathcal{C}_k^\alpha = 0$. As such, these states are *dark* because they do not contain photonic components, but also there is no optical transition to them from $|G\rangle$.

IV. The effective Hamiltonian and spectral density

Recall the total Hamiltonian reads as (c.f. Eq. S14)

$$\hat{H} = \sum_{j=1}^{N} \Big[\frac{\hat{P}_j^2}{2M} + V(\hat{R}_j)\Big] + \hat{H}_\nu + \frac{1}{2}\sum_{\mathbf{k}} \Big[\hat{p}_{\mathbf{k}}^2 + \omega_{\mathbf{k}}^2\Big(\hat{q}_{\mathbf{k}} + \frac{\lambda_{\mathrm{c}}}{\omega_{\mathbf{k}}}\sum_{j=1}^{N}\mu(\hat{R}_j)\cdot\cos\varphi_j\Big)^2\Big] + \hat{H}_{\mathrm{loss}}. \tag{S28}$$

It is shown that the the model Hamiltonian has a one-to-one map (through normal mode transformation) to the effective Hamiltonian as below,[12,13]

$$\hat{H} = \sum_{j=1}^{N} \Big[\frac{\hat{P}_j^2}{2M} + V(\hat{R}_j)\Big] + \hat{H}_\nu + \frac{1}{2}\sum_{\mathbf{k},\zeta} \Big[\hat{\tilde{p}}_j^2 + \tilde{\omega}_{\mathbf{k},\zeta}^2\Big(\hat{\tilde{x}}_{\mathbf{k},\zeta} - \frac{\tilde{c}_{\mathbf{k},\zeta}}{\tilde{\omega}_{\mathbf{k},\zeta}^2}\sum_{j=1}^{N}\mu(\hat{R}_j)\cdot\cos\varphi_j\Big)^2\Big], \tag{S29}$$

where the effective bath and its interaction with the system dissipation modes are described by an effective spectral density function,

$$J_{\mathrm{eff}}(\omega) \equiv \frac{\pi}{2}\sum_{\mathbf{k},\zeta}\frac{\tilde{c}_{\mathbf{k},\zeta}^2}{\tilde{\omega}_{\mathbf{k},\zeta}}\delta(\omega - \tilde{\omega}_{\mathbf{k},\zeta}). \tag{S30}$$

Note that the effective bath serves as the common bath for all the system DOFs. Now we provide a concise justification for this conclusion, and derive the explicit expression of the effective spectral density function. For convenience, we denote $\hat{\mathcal{S}} = \sum_{j=1}^{N}\mu(\hat{R}_j)\cdot\cos\varphi_j$ as the collective system dipole operator (which is equivalent to the $\hat{\mathcal{S}}_{\mathbf{k}}$ from Eq. S12b under the long-wavelength approximation). The terms in the total Hamiltonian (Eq. S28) that of interest for this normal mode transformation read as

$$\hat{H} - \hat{H}_\nu = \sum_{j=1}^{N}\left[\frac{\hat{P}_j^2}{2M} + V(\hat{R}_j)\right] + \frac{1}{2}\sum_{\mathbf{k}}\left[\hat{p}_{\mathbf{k}}^2 + \omega_{\mathbf{k}}^2\left(\hat{q}_{\mathbf{k}} + \frac{\lambda_{\mathrm{c}}}{\omega_{\mathbf{k}}}\hat{\mathcal{S}}\right)^2\right] + \frac{1}{2}\sum_{\mathbf{k},\zeta}\left[\hat{\tilde{p}}_{\mathbf{k},\zeta}^2 + \tilde{\omega}_{\mathbf{k},\zeta}^2\left(\hat{\tilde{x}}_{\mathbf{k},\zeta} - \frac{\tilde{c}_{\mathbf{k},\zeta}}{\tilde{\omega}_{\mathbf{k},\zeta}^2}\hat{q}_{\mathbf{k}}\right)^2\right], \tag{S31}$$

where $\hat{H}_\nu$ is omitted for not being directly involved in light-matter interactions. Next, by applying harmonic analysis to the equations of motion, we derive the effective spectral density function which describes the cavity modes as well as their associated loss. We will follow and generalize the approach proposed by Leggett[14] and Garg, et al.[12] The classical equations of motion with respect

to the Hamiltonian in Eq. S31 can be formally written down as

$$\ddot{\mathcal{S}} = -\frac{\partial V(\{R_j\})}{\partial \mathcal{S}} - \sum_{\mathbf{k}} \omega_{\mathbf{k}}^2 \cdot \frac{\lambda_{\mathrm{c}}}{\omega_{\mathbf{k}}} \left(q_{\mathbf{k}} + \frac{\lambda_{\mathrm{c}}}{\omega_{\mathbf{k}}} \mathcal{S} \right), \tag{S32a}$$

$$\ddot{q}_{\mathbf{k}} = -\omega_{\mathbf{k}}^2 \left(q_{\mathbf{k}} + \frac{\lambda_{\mathrm{c}}}{\omega_{\mathbf{k}}} \mathcal{S} \right) + \sum_{\zeta} \left(\tilde{c}_{\mathbf{k},\zeta} \tilde{x}_{\mathbf{k},\zeta} - \frac{\tilde{c}_{\mathbf{k},\zeta}^2}{\tilde{\omega}_{\mathbf{k},\zeta}^2} q_{\mathbf{k}} \right), \tag{S32b}$$

$$\ddot{\tilde{x}}_{\mathbf{k},\zeta} = -\tilde{\omega}_{\mathbf{k},\zeta}^2 \tilde{x}_{\mathbf{k},\zeta} + \tilde{c}_{\mathbf{k},\zeta} q_{\mathbf{k}}. \tag{S32c}$$

Applying Fourier transform to Eq. S32 leads to

$$\left(-\omega^2 + \sum_{\mathbf{k}} \lambda_{\mathrm{c}}^2 \right) \mathcal{S}(\omega) + \sum_{\mathbf{k}} \lambda_{\mathrm{c}} \omega_{\mathbf{k}} q_{\mathbf{k}}(\omega) = -V'_{\omega}, \tag{S33a}$$

$$\left[(\omega_{\mathbf{k}}^2 - \omega^2) + \sum_{j} \frac{\tilde{c}_{\mathbf{k},\zeta}^2}{\tilde{\omega}_{\mathbf{k},\zeta}^2} \right] q_{\mathbf{k}}(\omega) - \sum_{\zeta} \tilde{c}_{\mathbf{k},\zeta} \tilde{x}_{\mathbf{k},\zeta}(\omega) + \lambda_{\mathrm{c}} \omega_{\mathbf{k}} \mathcal{S}(\omega) = 0, \tag{S33b}$$

$$(-\omega^2 + \tilde{\omega}_{\mathbf{k},\zeta}^2) \tilde{x}_{\mathbf{k},\zeta}(\omega) - \tilde{c}_{\mathbf{k},\zeta} q_{\mathbf{k}}(\omega) = 0, \tag{S33c}$$

where V'_{ω} is the Fourier transform of $\partial V(\{R_j\})/\partial \mathcal{S}$. Plugging Eq. S33c into S33b to cancel the $\tilde{x}_{\mathbf{k},\zeta}(\omega)$ terms, one obtains

$$\left[\omega_{\mathbf{k}}^2 - \omega^2 \left(1 + \sum_{\zeta} \frac{\tilde{c}_{\mathbf{k},\zeta}^2}{\tilde{\omega}_{\mathbf{k},\zeta}^2 (-\omega^2 + \tilde{\omega}_{\mathbf{k},\zeta}^2)} \right) \right] q_{\mathbf{k}}(\omega) + \lambda_{\mathrm{c}} \omega_{\mathbf{k}} \mathcal{S}(\omega) = 0. \tag{S34}$$

We further define

$$L_{\mathbf{k}}(\omega) = -\omega^2 \left[1 + \sum_{\zeta} \frac{\tilde{c}_{\mathbf{k},\zeta}^2}{\tilde{\omega}_{\mathbf{k},\zeta}^2 (-\omega^2 + \tilde{\omega}_{\mathbf{k},\zeta}^2)} \right], \tag{S35}$$

Eq. S34 becomes

$$q_{\mathbf{k}}(\omega) = -\frac{\lambda_{\mathrm{c}} \omega_{\mathbf{k}} \mathcal{S}(\omega)}{\omega_{\mathbf{k}}^2 + L_{\mathbf{k}}(\omega)}. \tag{S36}$$

Notice that $L_{\mathbf{k}}(\omega)$ can be alternatively expressed as

$$L_{\mathbf{k}}(\omega) = -\omega^2 \left[1 + \int_0^{+\infty} ds \frac{\sum_\zeta \frac{\tilde{c}^2_{\mathbf{k},\zeta}}{\tilde{\omega}_{\mathbf{k},\zeta}} \delta(s - \tilde{\omega}_{\mathbf{k},\zeta})}{s(s^2 - \omega^2)} \right] = -\omega^2 \left[1 + \frac{2}{\pi} \int_0^{+\infty} ds \frac{J_{\text{loss}}(s, \mathbf{k})}{s(s^2 - \omega^2)} \right], \tag{S37}$$

where we used Eq. S10 to give rise to the loss spectral density function. Plugging Eq. S36 into S33a, one obtains

$$K(\omega)\mathcal{S}(\omega) \equiv \left(-\omega^2 + \sum_{\mathbf{k}} \frac{\lambda_{\text{c}}^2 L_{\mathbf{k}}(\omega)}{\omega_{\mathbf{k}}^2 + L_{\mathbf{k}}(\omega)} \right) \mathcal{S}(\omega) = -V'_\omega, \tag{S38}$$

And the total spectral density function felt by the reaction coordinate $\mathcal{S}$ is given by the branch cut of $K(z)$ on the complex plane, $J(\omega) = \lim_{\epsilon \to 0^+} \text{Im}[K(\omega - i\epsilon)]$. For our Eq. S38, it reads as[13,15]

$$J_{\text{eff}}(\omega) \equiv \frac{\pi}{2} \sum_{\mathbf{k},\zeta} \frac{\tilde{c}^2_{\mathbf{k},\zeta}}{\tilde{\omega}_{\mathbf{k},\zeta}} \delta(\omega - \tilde{\omega}_{\mathbf{k},\zeta}) = \sum_{\mathbf{k}} \frac{\lambda_{\text{c}}^2 \omega_{\mathbf{k}}^2 J_{\text{loss}}(\omega, \mathbf{k})}{\left[\omega_{\mathbf{k}}^2 - \omega^2 + \xi_{\mathbf{k}}(\omega)\right]^2 + \left[J_{\text{loss}}(\omega, \mathbf{k})\right]^2}, \tag{S39}$$

where $\xi_{\mathbf{k}}(\omega)$ is expressed as

$$\xi_{\mathbf{k}}(\omega) = \frac{2\omega^2}{\pi} \mathcal{P} \int_0^{\infty} ds \ \frac{J_{\text{loss}}(s, \mathbf{k})}{s(\omega^2 - s^2)}. \tag{S40}$$

And $\mathcal{P}$ in the above expression denotes to principal value integral. Notice that Eq. S39 is additive with respect to $\mathbf{k}$, meaning the total spectral density function is contributed by all of the cavity modes as well as their associated loss. Further, the normal mode transformations are restricted by the following identities,[13]

$$\lambda_{\text{c}} \omega_{\mathbf{k}} \hat{q}_{\mathbf{k}} = \sum_\zeta \tilde{c}_{\mathbf{k},\zeta} \hat{\tilde{x}}_{\mathbf{k},\zeta}, \qquad \sum_\zeta \tilde{c}^2_{\mathbf{k},\zeta} = \lambda_{\text{c}}^2 \omega_{\mathbf{k}}^2, \qquad \omega_{\mathbf{k}} = \lambda_{\text{c}}^2 \omega_{\mathbf{k}}^2 \cdot \left(\sum_\zeta \tilde{c}^2_{\mathbf{k},\zeta} / \tilde{\omega}^2_{\mathbf{k},\zeta} \right)^{-1}. \tag{S41}$$

To simplify our argument, we assume that the cavity loss is homogeneous (*i.e.*, does not depend on $\mathbf{k}$) and strictly Ohmic (*i.e.*, Markovian), which means

$$J_{\text{loss}}(\omega, \mathbf{k}) = \alpha\omega \exp(-\omega/\omega_{\text{m}}), \quad \omega_{\text{m}} \to +\infty, \tag{S42}$$

where $\alpha \equiv \tau_{\rm c}^{-1}$ is the inverse of the cavity lifetime $\tau_{\rm c}$. Under the Markovian limit, $\xi_{\mathbf{k}}(\omega) \to 0$, Eq. S39 is simplified as

$$J_{\rm eff}(\omega) = \sum_{\mathbf{k}} \frac{\lambda_{\rm c}^2 \omega_{\mathbf{k}}^2 \tau_{\rm c}^{-1} \omega}{\left(\omega_{\mathbf{k}}^2 - \omega^2\right)^2 + \tau_{\rm c}^{-2}\omega^2}, \tag{S43}$$

which is Eq. 10 of the main text.

V. The density of states and the effective spectral density

The cavity dispersion relation is written as (c.f. Eq. 2 of the main text)

$$\omega_{\mathbf{k}} = \frac{c}{n_{\rm c}}\sqrt{k_\perp^2 + k_\parallel^2} = \frac{ck_\perp}{n_{\rm c}}\sqrt{1+\tan^2\theta}. \tag{S44}$$

where $\tan\theta = k_\parallel/k_\perp$. In turn, one can calculate $k_\parallel$ in terms of the cavity frequency ω as

$$k_\parallel = \pm\frac{n_{\rm c}\sqrt{\omega_{\mathbf{k}}^2 - \omega_{\rm c}^2}}{c}, \tag{S45}$$

where for $k_\parallel = 0$ we introduce

$$\omega_{\rm c} = ck_\perp/n_{\rm c}, \tag{S46}$$

which is the photon frequency associated with the quantized direction (normal incidence). Evaluating the derivative of $k_\parallel$ with respect to ω, one obtains

$$\frac{dk_\parallel}{d\omega_{\mathbf{k}}} = \pm\frac{n_{\rm c}\omega_{\mathbf{k}}}{c\sqrt{\omega_{\mathbf{k}}^2 - \omega_{\rm c}^2}}. \tag{S47}$$

The density of states (DOS) is defined as

$$g(\omega) = \frac{c}{2n_{\rm c}k_\parallel^{\rm m}}\int_{-k_\parallel^{\rm m}}^{+k_\parallel^{\rm m}} \delta(\omega_{\mathbf{k}} - \omega)\; dk_\parallel = \frac{c}{2n_{\rm c}k_\parallel^{\rm m}}\int_0^{\omega_{\rm m}} \delta(\omega_{\mathbf{k}} - \omega)\frac{dk_\parallel}{d\omega_{\mathbf{k}}}d\omega_{\mathbf{k}} = \frac{\omega}{k_\parallel^{\rm m}\sqrt{\omega^2 - \omega_c^2}}\cdot\Theta(\omega - \omega_c), \tag{S48}$$

where $k_\parallel^{\mathrm{m}}$ is the cutoff value of the in-plane wavevector, $\omega_{\mathrm{m}} = \frac{c}{n_{\mathrm{c}}}\sqrt{k_\perp^2 + (k_\parallel^{\mathrm{m}})^2} \to \infty$ is the cutoff frequency, and $\Theta(\omega - \omega_{\mathrm{c}})$ is the Heaviside function, such that $\Theta(\omega - \omega_{\mathrm{c}}) = 1$ when $\omega \geq \omega_{\mathrm{c}}$ and $\Theta(\omega - \omega_{\mathrm{c}}) = 0$ when $\omega < \omega_{\mathrm{c}}$, such that there is no mode density below ω_c. Note that there is a singularity in the DOS at $\omega = \omega_{\mathrm{c}}$, which could play a crucial role in explaining the $k_\parallel$ dependence of VSC. Note that Eq. S48 can be equivalently expressed as

$$g(k_\parallel) = \frac{1}{k_\parallel^{\mathrm{m}}} \frac{\sqrt{k_\parallel^2 + k_\perp^2}}{k_\parallel} \cdot \Theta(\omega - \omega_c) = \frac{1}{2k_\parallel^{\mathrm{m}}} \sqrt{1 + \left(\frac{n_{\mathrm{c}}\omega_{\mathrm{c}}}{ck_\parallel}\right)^2}, \quad -k_\parallel^{\mathrm{m}} \leq k_\parallel \leq k_\parallel^{\mathrm{m}}, \tag{S49}$$

where under the limit of the $k_\parallel^{\mathrm{m}} \to \infty$, the above density of state reduces to

$$\lim_{k_\parallel^{\mathrm{m}} \to \infty} g(k_\parallel) \approx \delta(k_\parallel). \tag{S50}$$

One can easily check the normalization of $g(k_\parallel)$, which is $\int_{-k_\parallel^{\mathrm{m}}}^{k_\parallel^{\mathrm{m}}} dk_\parallel \; g(k_\parallel) = 1$. Equivalently, by defining the maximal incident angle θ_{m} via $k_\parallel^{\mathrm{m}} = k_\perp \tan\theta_{\mathrm{m}}$, and with $n_{\mathrm{c}}\omega_{\mathrm{c}}/ck_\parallel = k_\perp/k_\parallel = \cot\theta$, the density of state g can be expressed as a function of the incident angle θ as follows,

$$g(\theta) = \frac{1}{2k_\perp \tan\theta_{\mathrm{m}}} \sqrt{1 + \cot^2\theta}, \quad (\text{for } \; -\theta_{\mathrm{m}} \leq \theta \leq \theta_{\mathrm{m}}). \tag{S51}$$

It is easy to check that the normalization conditions

$$\int_0^{\omega_{\mathrm{m}}} d\omega \; (dk_\parallel/d\omega) g(\omega) = 1, \qquad \int_{-\theta_{\mathrm{m}}}^{\theta_{\mathrm{m}}} d\theta \; (dk_\parallel/d\theta) g(\theta) = 1 \tag{S52}$$

are both satisfied. The singularity of g appears at $k_\parallel = 0$ or $\theta = 0$, but the integral of it is finite and well-defined.

For a quasi-continuous wave vector $\mathbf{k}$, we can rewrite the summation in Eq. S39 into integration. The integration measure should be chosen as $dk_\parallel$ as it is physically expected, which means varying $k_\parallel$ evenly. Here, we convert it to $d\theta$ via chain rule, and every $\mathbf{k}$-dependent term is expressed in terms of θ. Recall that we derived the DOS of the Fabry-Pérot cavity as (c.f. Eq. S51)

$$g(\theta) = \frac{1}{2k_\perp \tan\theta_{\mathrm{m}}} \sqrt{1 + \cot^2\theta}, \quad -\theta_{\mathrm{m}} \leq \theta \leq \theta_{\mathrm{m}}, \quad \theta_{\mathrm{m}} \to \frac{\pi}{2}, \tag{S53}$$

which will reduce to a δ-function $\delta(\theta)/k_\perp$ when $\theta_\mathrm{m} \to \pi/2$. And the dispersion relation is (c.f. Eq. S44)

$$k_\parallel = k_\perp \tan\theta, \qquad \omega_\mathbf{k} = \omega_\mathrm{c}\sqrt{1+\tan^2\theta}. \tag{S54}$$

As a result, Eq. S39 becomes

$$\begin{aligned} J_\mathrm{eff}(\omega) &= \int_{-k_\parallel^\mathrm{m}}^{k_\parallel^\mathrm{m}} dk_\parallel \; g(\theta) \frac{\lambda_\mathrm{c}^2 \omega_\mathbf{k}^2 \tau_\mathrm{c}^{-1}\omega}{\left(\omega_\mathbf{k}^2-\omega^2\right)^2+\tau_\mathrm{c}^{-2}\omega^2} \\ &= \frac{\omega_\mathrm{c}^2\lambda_\mathrm{c}^2}{2k_\perp\tan\theta_\mathrm{m}} \int_{-\theta_\mathrm{m}}^{\theta_\mathrm{m}} d\theta \; \frac{dk_\parallel}{d\theta}\sqrt{1+\cot^2\theta} \cdot \frac{(1+\tan^2\theta)\tau_\mathrm{c}^{-1}\omega}{\left(\omega_\mathbf{k}^2-\omega^2\right)^2+\tau_\mathrm{c}^{-2}\omega^2} \\ &= \frac{\omega_\mathrm{c}^2\lambda_\mathrm{c}^2}{\tan\theta_\mathrm{m}} \int_0^{\theta_\mathrm{m}} d\theta \; \frac{\sqrt{1+\cot^2\theta}}{\cos^4\theta} \cdot \frac{\tau_\mathrm{c}^{-1}\omega}{\left(\omega_\mathbf{k}^2-\omega^2\right)^2+\tau_\mathrm{c}^{-2}\omega^2}, \end{aligned} \tag{S55}$$

which is Eq. 12 of the main text. Here, we take the limit of $\theta_\mathrm{m} \to \pi/2$, so that the DOS will reduce to $\delta(\theta)/k_\perp$ (see Eq. S49). As a result, one can obtain from Eq. S55 that

$$J_\mathrm{eff}(\omega) = \omega_\mathrm{c}^2\lambda_\mathrm{c}^2 \cdot \frac{\tau_\mathrm{c}^{-1}\omega}{\left(\omega_\mathrm{c}^2-\omega^2\right)^2+\tau_\mathrm{c}^{-2}\omega^2}, \tag{S56}$$

which is Eq. 13 of the main text. Note that Eq. S56 reduces to the single mode case. The validation of single-mode approximation in the VSC problem will greatly benefit us to simplify the analysis. Physically, it means that the DOS at $\theta \neq 0$ is infinitesimal compared to the DOS at $\theta = 0$. But this is not contrary to the fact that there is still Rabi-splitting when $\omega_0 > \omega_\mathrm{c}$ because there are indeed modes (and associated photonic states) at that higher frequency.

VI. Derivation of $\tilde{k}_\mathrm{VSC}$ (Eq. 19 of the main text)

Here, we theoretically justify Eq. 19 of the main text, for the general case of τ_c dependence. In the case of a very large τ_c, the leading term that causes the broadening of the $|\nu_\mathrm{L}^j\rangle \to |\nu_\mathrm{L}'^j\rangle$ transition comes from the $\hat{H}_\nu$ term in Eq. S3, which must then be considered in the rate expression. This is a Holstein-type system-bath coupling (diagonal coupling) and is identical for all molecules $j \in [1, N]$,

which is expressed as

$$\left[R_{\mathrm{LL}}|\nu_{\mathrm{L}}^{j}\rangle\langle\nu_{\mathrm{L}}^{j}| + R_{\mathrm{L'L'}}|\nu_{\mathrm{L}}^{\prime j}\rangle\langle\nu_{\mathrm{L}}^{\prime j}|\right] \otimes \hat{F}_{\nu}^{j} \equiv \epsilon_z \cdot \frac{1}{2}\sigma_z^j \otimes \hat{F}_{\nu}^{j}, \tag{S57}$$

where $R_{\mathrm{LL}} = \langle\nu_{\mathrm{L}}^{j}|\hat{R}_j|\nu_{\mathrm{L}}^{j}\rangle$, similar for $R_{\mathrm{L'L'}}$, and the stochastic force operator of the phonon is

$$\hat{F}_{\nu}^{j} = \sum_{\zeta} c_\zeta \hat{x}_{j,\zeta}. \tag{S58}$$

Further, $\hat{\sigma}_z^j = |\nu_{\mathrm{L}}^{\prime j}\rangle\langle\nu_{\mathrm{L}}^{\prime j}| - |\nu_{\mathrm{L}}^{j}\rangle\langle\nu_{\mathrm{L}}^{j}|$, and $\epsilon_z = R_{\mathrm{LL}} - R_{\mathrm{L'L'}} = 9.39$ a.u. for the model system considered in Sec. II. Eq. S57 is mainly responsible for the inhomogeneous broadening effect in the spectra, and it should also broaden the transition frequency ω_0. The variance of this fluctuation term is[16–18]

$$\sigma^2 = \epsilon_z^2 \cdot \frac{1}{\pi}\int_0^\infty d\omega\ J_\nu(\omega)\coth(\beta\omega/2), \tag{S59}$$

where $J_\nu(\omega)$ is identical for all molecules. With the above analysis, the rate constant in a general form can be written down as the following convolution expression[19]

$$\tilde{k}_{\mathrm{VSC}} = \int_0^\infty d\omega\ k_{\mathrm{VSC}}(\omega)G(\omega-\omega_0), \tag{S60}$$

where the broadening function $G(\omega-\omega_0)$ is a Gaussian distribution centered around ω_0, defined as

$$G(\omega-\omega_0) = \frac{1}{\sqrt{2\pi\sigma^2}}\exp\left[-\frac{(\omega-\omega_0)^2}{2\sigma^2}\right], \tag{S61}$$

with the width expressed in Eq. S59. This is the result of Eq. 19 of the main text.

There are several interesting limits of the expression in Eq. S60. First, in the lossless limit ($\tau_{\mathrm{c}} \to \infty$) and the effective spectral density function in Eq. S56 (Eq. 13 of the main text) will reduce to a single δ-function, $J_{\mathrm{eff}}(\omega) \approx \frac{\pi}{2}\lambda_{\mathrm{c}}^2\omega_{\mathrm{c}}\delta(\omega-\omega_{\mathrm{c}})$. As a result, the broadening is fully dictated by the variance of the Gaussian. If we focus on the case of fully isotropic dipoles, then

$$\tilde{k}_{\mathrm{VSC}} \approx \frac{2\pi}{3}\cdot N g_{\mathrm{c}}^2\omega_{\mathrm{c}} n(\omega_0)\cdot\int_0^\infty d\omega\ \delta(\omega-\omega_{\mathrm{c}})G(\omega-\omega_0) = \frac{2\pi}{3}\cdot N g_{\mathrm{c}}^2\omega_{\mathrm{c}}\cdot G(\omega_{\mathrm{c}}-\omega_0)\cdot e^{-\beta\hbar\omega_0} \tag{S62}$$

The rate profile described in Eq. S62 is a Gaussian function centered at ω_0 with respect to cavity frequency ω_c. This expression is valid for an arbitrarily high-Q cavity with lifetime $\tau_c \to \infty$, and the resonant behavior is apparently enforced by the Gaussian function, where the maximum of the rate is reached when $\omega_c = \omega_0$. Note that under this limit, the rate profile is purely controlled by the broadening σ (see Eq. S59), which is related to the phonon spectral density $J_\nu(\omega)$. In general, there is still the broadening effect due to the τ_c^{-1} term in $J_{\text{eff}}(\omega)$, but less significant. To numerically show the effects of cavity lifetime, we follow Ref. 10 by setting the phonon bath of $\hat{H}_\nu$ as the Drude-Lorentz form, $J_\nu(\omega) = 2\lambda\gamma\omega/(\omega^2 + \gamma^2)$, where λ is the reorganization energy, γ is the characteristic frequency. Unfortunately, the integral in Eq. S59 is divergent for the Drude-Lorentz spectral density, so we instead take the upper limit of the integral to be the characteristic frequency γ (which is in line with the *low frequency modes* that bring about static disorder). Here we take $\gamma = 200$ cm^{-1}, and $\lambda = 0.1\omega_b\gamma/2$ (the same set up as Ref. 10). The numerical value of the broadening factor at $T = 300$ K is $\sigma = 29.24$ cm^{-1}.

Second, under the limit when the phonon broadening is much smaller than the cavity caused broadening, which happens when $\tau_c^{-1} \gg \sigma$ (for example, when $\tau_c \to 0$), the Gaussian function $G(\omega - \omega_0)$ is then much narrower than the $J_{\text{eff}}(\omega)$, such that we can approximate $G(\omega - \omega_0)$ as a single δ-function, $G(\omega - \omega_0) \approx \delta(\omega - \omega_0)$, then the k_{VSC} expression in Eq. S60 becomes

$$\tilde{k}_{\text{VSC}} \approx k_{\text{VSC}}(\omega_0), \tag{S63}$$

such that the cavity-related width $\Gamma_c = \tau_c^{-1}$ dominates the rate profile. Under this limit, the rate reduces to the expressions presented in the main text: Eq. 14 for the coherent picture of FGR and Eq. 15 for the incoherent picture of FGR.

VII. Details of the Numerical Results in Fig. 3

We provide details of the numerical results presented in Fig. 3 of the main text, to illustrate the VSC resonance phenomena, and how the VSC-caused rate constant change k_{VSC} is influenced by light-matter coupling strength (Rabi-splitting Ω_R) and cavity lifetime τ_c. The model parameters are provided in Table 1 in Sec. II. To simplify our argument, k_{VSC} is calculated using Eq. 17 of

the main text for the *fully aligned case* because we can directly relate the coupling strength to the Rabi splitting.

Fig. 1a presents k_{VSC} as a function of ω_{c}. The rate profile peaks at $\omega_{\mathrm{c}} = \omega_0$. As one increases the light-matter coupling strength, or the Rabi splitting Ω_{R}, the magnitude of the change also increases, but they all have a similar sharp-resonance profile. Fig. 1b presents the value of $k/k_0 = 1 + k_{\mathrm{VSC}}/k_0$ at $\omega_{\mathrm{c}} = \omega_0$, as a function of Ω_{R} (red curve), reading with the y-axis on the right-hand side. The value of k_0 needs to be computed separately, where we use $k_0 = 2.3 \times 10^{-6}$ fs^{-1}, obtained from the previous exact quantum dynamics simulations[10] for the same ground-state reaction model investigated here. The overall scaling is quadratic with Rabi splitting,

$$k/k_0 \propto 1 + \mathcal{C} \cdot \left(\Omega_{\mathrm{R}}/2\omega_{\mathrm{c}}\right)^2 , \tag{S64}$$

where $\mathcal{C}$ is a constant factor.

Fig. 1b further presents the effective change of the free energy barrier $\Delta(\Delta G^{\ddagger})$ (blue), directly backed out from the rate constants ratio k/k_0. To account for the "effective change" of the Gibbs free energy barrier $\Delta(\Delta G^{\ddagger})$, we consider the simple rate equation[11] inside the cavity as $k = A \cdot \exp\left[-\Delta G^{\ddagger}/k_{\mathrm{B}}T\right]$, and outside the cavity case as $k_0 = A \cdot \exp\left[-\Delta G_0^{\ddagger}/k_{\mathrm{B}}T\right]$, as is commonly assumed by experimental analysis.[11,20] The pre-factor A is assumed to be the same with or without the cavity. The change of free energy barrier compared to the bare molecular reaction (with k_0 and $\Delta G_0^{\ddagger}$) is then

$$\Delta(\Delta G^{\ddagger}) = \Delta G^{\ddagger} - \Delta G_0^{\ddagger} = -k_{\mathrm{B}}T \ln\left(k/k_0\right). \tag{S65}$$

Note that this is not an actual free energy barrier change, but rather a purely kinetic effect (as we best understood, through the FGR in Eq. 14, Eq. 17, and Eq. 18 of the main text). Based on Eq. S64, we *predict* that

$$\Delta(\Delta G^{\ddagger}) \propto -k_{\mathrm{B}}T \ln\left[1 + \mathcal{C} \cdot \left(\Omega_{\mathrm{R}}/2\omega_{\mathrm{c}}\right)^2\right]. \tag{S66}$$

Note that if one hypothesizes that an unknown mechanism forces the upper or lower vibrational polariton states to be a "gateway of VSC polaritonic" chemical reaction,[21] then the activation free energy change should shift linearly[22] with Ω_{R}. The experimental results, on the other hand, demon-

strate a non-linearity of reaction barrier.[11,20] Our current theory predicts a non-linear increase of the "effective" $\Delta(\Delta G^{\ddagger})$ in Eq. S66 as increasing $\Omega_{\rm R}$ due the cavity promotion of the $|\nu_{\rm L}\rangle \to |\nu'_{\rm L}\rangle$ transition, and more particularly, the effective $\Delta(\Delta G^{\ddagger})$ scales with $-k_{\rm B}T\ln\left[1+\mathcal{C}\cdot(\Omega_{\rm R}/2\omega_{\rm c})^2\right]$. Further, in Ref. 23, it was pointed out that for a very small Rabi splitting ($\Omega_{\rm R} = 100$ cm^{-1}) observed in optical spectra, it can lead to much larger changes in activation free energy $\Delta(\Delta G^{\ddagger}) \approx 0.8$ kcal/mol or 3.3 kJ/mol), such that $\Delta(\Delta G^{\ddagger}) > \Omega_{\rm R}$. This seems to be a general trend in most VSC experiments,[11] but it lacks a theoretical explanation. Here, we provide one due to the FGR nature of the rate constant, which significantly influences the rate and correspondingly, the effective free energy barrier.

Fig. S1a presents $\tilde{k}_{\rm VSC}$ as a function of cavity frequency $\omega_{\rm c}$, as well as cavity lifetime $\tau_{\rm c}$, by numerically evaluating Eq. S62 and the model spectral density $J_\nu(\omega)$ mentioned in section VI. Decreasing $\tau_{\rm c}$ leads to a weakening and broadening of the resonance peak of the rate profile. The cavity modification effect gradually disappears at the heavy loss limit $\tau_{\rm c} \to 0$. To the best of our knowledge, there is no existing experiment that directly verifies the $\tau_{\rm c}$-dependence of the VSC effect. Future experimental efforts could be dedicated to this specific check. Fig. S1b, which is the identical plot of Fig. 3c in the main text, presents the value of k/k_0 at $\omega_{\rm c} = \omega_0$, as a function of $\tau_{\rm c}$ (on a log scale in $\tau_{\rm c}$). The rate constant modification changes in a sigmoid trend, which is subject to future experimental verification.

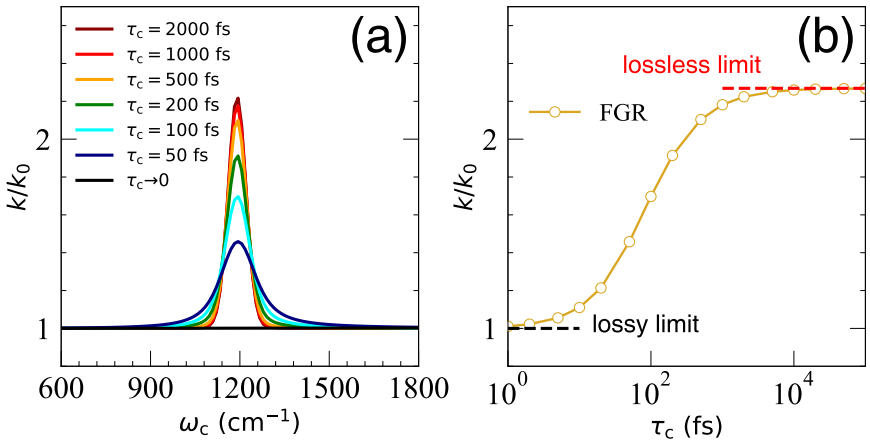

Figure S1: (a) Effect of $\tau_{\rm c}$ on the rate constant ratio k/k_0. Note that the cavity modification effects become smaller when $\tau_{\rm c}$ is reduced and under the heavy loss limit ($\tau_{\rm c} \to 0$) the cavity effect vanishes. (b) The peak value of k/k_0 (at $\omega_{\rm c} = \omega_0$ as a function of cavity life time $\tau_{\rm c}$. The Rabi-splitting is fixed at $\hbar\Omega_{\rm R} = 100$ cm^{-1}.

References

(1) Power, E. A.; Zienau, S. Coulomb gauge in non-relativistic quantum electro-dynamics and the shape of spectral lines. *Philos. Trans. Royal Soc. A* **1959**, *251*, 427–454.

(2) Cohen-Tannoudji, C.; Dupont-Roc, J.; Grynberg, G. *Photons and Atoms: Introduction to Quantum Electrodynamics*; Wiley, 1997.

(3) Woolley, R. G. A reformulation of molecular quantum electrodynamics. *J. Phys. B: At. Mol. Phys.* **1974**, *7*, 488–499.

(4) Mandal, A.; Taylor, M.; Weight, B.; Koessler, E.; Li, X.; Huo, P. Theoretical Advances in Polariton Chemistry and Molecular Cavity Quantum Electrodynamics. *ChemRxiv* **2022**,

(5) Keeling, J. *Light-Matter Interactions and Quantum Optics*; University of St. Andrews, 2012.

(6) Caldeira, A.; Leggett, A. Quantum tunnelling in a dissipative system. *Ann. Physics* **1983**, *149*, 374–456.

(7) Topaler, M.; Makri, N. Quantum rates for a double well coupled to a dissipative bath: Accurate path integral results and comparison with approximate theories. *J. Chem. Phys.* **1994**, *101*, 7500–7519.

(8) Shi, Q.; Zhu, L.; Chen, L. Quantum rate dynamics for proton transfer reaction in a model system: Effect of the rate promoting vibrational mode. *J. Chem. Phys.* **2011**, *135*, 044505.

(9) Colbert, D. T.; Miller, W. H. A novel discrete variable representation for quantum mechanical reactive scattering via the S-matrix Kohn method. *J. Chem. Phys.* **1992**, *96*, 1982–1991.

(10) Lindoy, L. P.; Mandal, A.; Reichman, D. R. Quantum dynamical effects of vibrational strong coupling in chemical reactivity. *Nat. Commun.* **2023**, *14*, 2733.

(11) Thomas, A.; Jayachandran, A.; Lethuillier-Karl, L.; Vergauwe, R. M.; Nagarajan, K.; Devaux, E.; Genet, C.; Moran, J.; Ebbesen, T. W. Ground state chemistry under vibrational strong coupling: dependence of thermodynamic parameters on the Rabi splitting energy. *Nanophotonics* **2020**, *9*, 249–255.

(12) Garg, A.; Onuchic, J. N.; Ambegaokar, V. Effect of friction on electron transfer in biomolecules. *J. Chem. Phys.* **1985**, *83*, 4491–4503.

(13) Thoss, M.; Wang, H.; Miller, W. H. Self-consistent hybrid approach for complex systems: Application to the spin-boson model with Debye spectral density. *J. Chem. Phys.* **2001**, *115*, 2991–3005.

(14) Leggett, A. J. Quantum tunneling in the presence of an arbitrary linear dissipation mechanism. *Phys. Rev. B* **1984**, *30*, 1208–1218.

(15) Lawrence, J. E.; Fletcher, T.; Lindoy, L. P.; Manolopoulos, D. E. On the calculation of quantum mechanical electron transfer rates. *J. Chem. Phys.* **2019**, *151*, 114119.

(16) Troisi, A.; Nitzan, A.; Ratner, M. A. A rate constant expression for charge transfer through fluctuating bridges. *J. Chem. Phys.* **2003**, *119*, 5782–5788.

(17) Castellanos, M. A.; Huo, P. Enhancing Singlet Fission Dynamics by Suppressing Destructive Interference between Charge-Transfer Pathways. *J. Phys. Chem. Lett.* **2017**, *8*, 2480–2488.

(18) Chowdhury, S. N.; Mandal, A.; Huo, P. Ring polymer quantization of the photon field in polariton chemistry. *J. Chem. Phys.* **2021**, *154*, 044109.

(19) Mukamel, S. *Principles of Nonlinear Optical Spectroscopy*; Oxford University Press, 1995.

(20) Lather, J.; Bhatt, P.; Thomas, A.; Ebbesen, T. W.; George, J. Cavity Catalysis by Cooperative Vibrational Strong Coupling of Reactant and Solvent Molecules. *Angew. Chem. Int. Ed.* **2019**, *58*, 10635–10638.

(21) Hiura, H.; Shalabney, A.; George, J. A Reaction Kinetic Model for Vacuum-Field Catalysis Based on Vibrational Light-Matter Coupling. *ChemRxiv* **2019**,

(22) Li, T. E.; Nitzan, A.; Subotnik, J. E. On the origin of ground-state vacuum-field catalysis: Equilibrium consideration. *J. Chem. Phys.* **2020**, *152*, 234107.

(23) Hirai, K.; Hutchison, J. A.; Uji-i, H. Recent Progress in Vibropolaritonic Chemistry. *ChemPlusChem* **2020**, *85*, 1981–1988.